

The strong coupling from hadronic τ -decay data including $\tau \rightarrow \pi^- \pi^0 \nu_\tau$ from Belle

Diogo Boito,^a Aaron Eiben,^b Maarten Golterman,^b Kim Maltman,^{c,d}
Lucas M. Mansur,^a and Santiago Peris^e

^aInstituto de Física de São Carlos, Universidade de São Paulo, CP 369, 13560-970, São Carlos, SP, Brazil

^bDepartment of Physics and Astronomy, San Francisco State University,
San Francisco, CA 94132, USA

^cDepartment of Mathematics and Statistics, York University
Toronto, ON Canada M3J 1P3

^dCSSM, University of Adelaide, Adelaide, SA 5005 Australia

^eDepartment of Physics and IFAE-BIST, Universitat Autònoma de Barcelona
E-08193 Bellaterra, Barcelona, Spain

In previous work we have combined the $\pi^- \pi^0$, $2\pi^- \pi^+ \pi^0$ and $\pi^- 3\pi^0$ spectral data obtained from hadronic τ decays measured by the ALEPH and OPAL experiments, together with electroproduction data for several of the subleading hadronic modes and BaBar data for the $K \bar{K}$ mode to construct an inclusive non-strange vector spectral function entirely based on experimental data, with no Monte-Carlo generated input. In this paper, we include, for the first time, the Belle $\tau \rightarrow \pi^- \pi^0 \nu_\tau$ high-statistics decay data to construct a new inclusive non-strange vector spectral function that combines more of the world's available data. As no Belle data are at present available for the two 4π modes, this requires a revised data analysis in comparison with our previous work. From the resulting new spectral function, we obtain a new determination of the strong coupling, α_s , using our previously developed strategy based on finite-energy sum rules. We find, at the Z mass scale, $\alpha_s(m_Z^2) = 0.1159(14)$. We discuss the smaller central value and larger error of our new result compared to our previous result, showing the shifts to be due mainly to significant changes in updated HFLAV results for the $\pi^- 3\pi^0$ decay mode.

I. INTRODUCTION

There has been a longstanding interest in the determination of the strong coupling, α_s , from hadronic τ decays. There are two main reasons for this: first, the value obtained from τ decays is among the more precise ones [1], and second, it provides a valuable test of our understanding of its running as predicted by QCD because all other precise determinations have been obtained at considerably larger scales.

In this paper, we will be concerned with the determination of α_s from τ decays in the non-strange vector (V) channel. There are several experiments that have obtained data for hadronic τ decays. The LEP experiments ALEPH [2–4] and OPAL [5] produced results for the fully inclusive non-strange (isovector) V spectral function obtained by supplementing measured contributions from the dominant decay modes, $\pi^-\pi^0$, $2\pi^-\pi^+\pi^0$ and $\pi^-3\pi^0$, with those from a number of additional exclusive modes with small branching fractions (BFs) estimated using Monte-Carlo simulations. More recently, the KEK-based Belle experiment [6] has produced results for the contribution to the spectral function of the $\pi^-\pi^0$ exclusive mode, which has the largest of the V channel hadronic BFs. Information on this mode is also available from CLEO [7, 8].

Clearly, a robust determination of α_s should make use of the world’s data on hadronic τ decays, after investigating whether the available data sets are statistically compatible. In previous work [9] we combined the ALEPH and OPAL data for the $\pi^-\pi^0$, $2\pi^-\pi^+\pi^0$ and $\pi^-3\pi^0$ modes (which we will refer to as the $2\pi + 4\pi$ data) into a three-mode-summed $2\pi + 4\pi$ spectral function contribution. By BF, these three modes constitute about 98% of the inclusive non-strange V channel contribution to hadronic τ decays. We then used for the $K\bar{K}$ spectral contributions recent BaBar differential $\tau \rightarrow K\bar{K}\nu_\tau$ [10] distribution results, and for the contributions from the remaining modes, $\pi^-\omega(\rightarrow \text{non-}3\pi)$ [11, 12], $\eta\pi^-\pi^0$ [13–18], $K\bar{K}\pi$ [19], 6π [20–25], $K\bar{K}\pi\pi$ [19], $(3\pi)^-\omega(\rightarrow \text{non-}3\pi)$ [20], $\pi^-\eta\omega(\rightarrow \text{non-}3\pi)$ [26] and $\eta 4\pi$ [26, 27], results obtained using electroproduction cross section data in combination with the CVC (Conserved Vector Current) relation.¹ The contributions from these modes had previously been estimated using input from Monte-Carlo simulations. Exclusive-mode τ -decay BFs were obtained from Ref. [28] where needed. These additions produced an inclusive non-strange V channel spectral function with experimental data used for exclusive-mode contributions representing at least 99.95% by BF of the inclusive non-strange V total, removing the need for Monte-Carlo input.

Because of significantly increased statistics relative to the LEP-based experiments, the errors on the unit-normalized Belle $\pi^-\pi^0$ data are much smaller than those of ALEPH and OPAL, and it thus makes sense to combine the $\pi^-\pi^0$ data of all three experiments with the aim of increasing the overall precision of the non-strange V inclusive spectral function. Including the Belle data is thus one of the main goals of this paper. The possibility of including the older CLEO $\pi^-\pi^0$ data in this combination is also considered, though this is hampered by the lack of complete information on the CLEO systematic errors.

The inclusion of the Belle $\pi^-\pi^0$ data requires a complete redesign of the algorithm employed in our previous $2\pi + 4\pi$ data combination based on the ALEPH and OPAL data. The reason is that in Ref. [9] we first added the $\pi^-\pi^0$ and two 4π contributions for each of ALEPH and OPAL separately (using BFs from Ref. [28]) before forming the two-experiment, three-mode sum, instead of first combining ALEPH and OPAL contributions for each of the three

¹ We follow Ref. [9] in referring to exclusive modes other than 2π and 4π as “residual modes.” See Ref. [9] for the complete analysis of these residual-mode contributions.

modes separately and then combining those results into the two-experiment, three-mode sum. The reason for this choice was that the covariance matrices of the separate ALEPH and OPAL $2\pi^-\pi^+\pi^0$ and $\pi^-3\pi^0$ contributions to the unit-normalized exclusive-mode spectral function are poorly determined, but adding the three contributions for each experiment first made the combined $2\pi + 4\pi$ covariance matrices well-behaved for both ALEPH and OPAL, thus allowing us to combine the two $2\pi + 4\pi$ data sets.² Clearly, this procedure needs to be revised when the Belle $\pi^-\pi^0$ data are included in the combination as well.

The modification of our strategy to allow for the inclusion of the Belle $\pi^-\pi^0$ data set, also, in principle, allows us to include the older CLEO $\pi^-\pi^0$ data set [7, 8]. Although CLEO provided a careful estimate of systematic errors for integrated quantities such as a_μ^{HVP} , the hadronic vacuum polarization contribution to the muon anomalous magnetic moment, a covariance matrix for the systematic errors bin-by-bin was not provided.³ We have, nonetheless, also investigated the effect of including the CLEO $\pi^-\pi^0$ data, verifying its consistency with the results from the other experiments. Since, however, the information on the CLEO systematic uncertainties is less complete than that for the other three experiments, the quantitative results of this exploration are not taken into account in obtaining the main results of this paper.

The data combination we performed in our previous work [9] employed the algorithm of Ref. [29], in which the experimental data is divided among a number of “clusters.” The combined spectral function is then defined by interpolation between the cluster values, which, in turn, are fitted to the experimental data. A detailed description of this procedure is provided in Sec. III B.

The strategy we adopt here can be summarized as follows. We first carry out the $\pi^-\pi^0$ combination using ALEPH, OPAL and Belle unit-normalized data, following the algorithm of Ref. [29], and then multiply the result with the BF from the updated HFLAV analysis [30]. We then consider the ALEPH and OPAL 4π data in more detail. The covariance matrix for the OPAL $\pi^-3\pi^0$ data is particularly badly behaved, because of large backgrounds (in particular from other modes with one π^- , such as $\pi^-\pi^0$ and $\pi^-2\pi^0$) making it difficult to reliably determine the $\pi^-3\pi^0$ covariances [5].⁴ To deal with this problem, we include only the diagonal entries of the OPAL $\pi^-3\pi^0$ covariance matrix in our fit combining the ALEPH and OPAL 4π data, while using the full covariance matrix for error propagation. Doing so, we found that, if we combine the two 4π modes for each of ALEPH and OPAL first, we can carry out a pure- 4π fit to these data, thus obtaining a combined ALEPH plus OPAL two-mode, 4π spectral function contribution. Finally, we add the combined 2π and combined 4π spectral function contributions (*c.f.* Sec. III E). While correlations between different modes have not been provided by the ALEPH and OPAL experiments, we take into account the small correlations induced by the correlations between the BFs of the three modes as provided by HFLAV [30].

The contribution from the residual modes will be taken in unmodified form from Ref. [9] because any more recent updates of τ BFs and/or the relevant exclusive-mode electroproduction cross sections do not affect our results within errors. We remind the reader that isospin breaking associated with the use of CVC for contributions obtained using electroproduction data and CVC are too small to have any effect, since contributions from these modes lie at squared invariant masses well above the $\rho-\omega$ resonance region. Isospin-breaking corrections

² The three-mode sum is dominated by $\pi^-\pi^0$ contributions, for which the ALEPH and OPAL covariance matrices are well known and well behaved.

³ We thank Jon Urheim for an email exchange on this topic.

⁴ We thank Sven Menke for an email exchange on this topic.

to these contributions will thus receive no narrow, nearby $I = 0/1$ resonance interference enhancements, and hence are expected to be at the $O(1\%)$ (or less) level, much smaller than the errors on the CVC-converted contributions. Adding the residual-mode and $2\pi + 4\pi$ contributions we obtain a new inclusive non-strange, vector-isovector spectral function which now includes the Belle $\pi^-\pi^0$ data.

In the second part of this paper, we use finite-energy sum rules (FESRs) to fit α_s to moments of the new non-strange V spectral function. To do this, we follow the strategy of Ref. [9], comparing our results with those obtained in that earlier work. In this strategy, non-perturbative effects are taken into account through the operator product expansion (OPE) and a model for quark-hadron duality violations (DVs). This strategy is fundamentally different from the alternate “truncated OPE” (tOPE) approach used in a number of earlier analyses in the literature Refs. [2–5, 31–34]. Within the tOPE, α_s turns out to be determined from FESRs involving high-degree polynomial weights in which only perturbative contributions are retained in the corresponding theoretical representations [37]. The neglect of in-principle-present non-perturbative (NP) contributions (in particular those proportional to higher-dimension OPE condensates) is potentially dangerous at scales as low as the τ mass. In Ref. [37], for example, it was shown that a V -channel optimal-weight tOPE analysis at a scale $s_0 = 2.88 \text{ GeV}^2$ (which is slightly higher than that employed in the ALEPH-based V -channel tOPE analyses of Refs. [33, 34]), based on the improved V spectral function of Ref. [9], produced a discrepancy larger than 6σ between the two single-weight α_s determinations obtained from the underlying NP-free FESRs, leading to a very large $\chi^2/\text{dof} \simeq 43/1$ for the fit combining these two NP-free FESRs. Since similarly large χ^2 are found for $s_0 \simeq 2.88 \text{ GeV}^2$ tOPE analyses of the types employed in Refs. [33, 34] employing the improved V -channel spectral function constructed in the present paper, we do not consider further the tOPE approach in what follows.⁵

In the (dominant) perturbative part of our FESR-based analysis, we use the results of Ref. [32] in the standard $\overline{\text{MS}}$ scheme, which, in the context of FESRs, is usually referred to as fixed-order perturbation theory (FOPT). The alternative approach based on a resummation known as contour-improved perturbation theory (CIPT) [38, 39] was recently shown to be inconsistent with the standard OPE [40–44] and will thus not be employed.

This paper is organized as follows. In Sec. II we briefly summarize the FESRs that allow us to extract α_s from the inclusive non-strange V spectral function. Section III is devoted to the construction of the new spectral function. In particular, in this section we explain our strategy for combining the ALEPH and OPAL 4π data, and adding this to the combined 2π data and the residual-mode data from Ref. [9] to arrive at a new inclusive result that now also includes the $\pi^-\pi^0$ data from Belle. In Sec. IV, we use the framework of Sec. II to produce our new result for α_s at the τ mass. Section V contains our conclusions. There are three appendices. The first details our handling of the d’Agostini bias [45] in the 4π data combination step, and the second one summarizes a study of the effects of including the CLEO $\pi^-\pi^0$ data set in addition to those of ALEPH, OPAL and Belle. The third one contains details on combining the 2π and 4π spectral functions.

⁵ We refer to Refs. [35–37] for a more detailed assessment of the tOPE approach.

II. THEORY REVIEW

Our theoretical framework for the determination of $\alpha_s(m_\tau^2)$ from the inclusive non-strange V spectral function is the same as that of Ref. [9], and we will therefore be very brief. More details can also be found in earlier work, notably in the first paper in which we employed this strategy, Ref. [46], but see also Refs. [47, 48].

A. Finite energy sum rules

As we will only consider the non-strange V channel in this paper, we will limit our review to that case. The key object entering the analysis of this channel is the spin-1 scalar vacuum polarization, $\Pi^{(1)}$, of the isovector, V current-current two-point function. Neglecting the very small up-down quark mass difference, the two-point function is purely transverse and related to $\Pi^{(1)}$ by

$$\Pi_{\mu\nu}(q) = i \int d^4x e^{iqx} \langle 0 | T \{ J_\mu(x) J_\nu^\dagger(0) \} | 0 \rangle = (q_\mu q_\nu - q^2 g_{\mu\nu}) \Pi^{(1)}(q^2) , \quad (2.1)$$

where J_μ is the isovector V current $\bar{u}\gamma_\mu d$. $\Pi^{(1)}$ is also dispersively related to the corresponding spin-1 spectral function,

$$\rho^{(1)}(s) = \frac{1}{\pi} \text{Im} \Pi^{(1)}(s) , \quad (2.2)$$

with $s = q^2$. $\Pi^{(1)}$ and $\rho^{(1)}$ satisfy the Cauchy Theorem (FESR) relation,

$$I^{(w)}(s_0) \equiv \frac{1}{s_0} \int_0^{s_0} ds w(s) \rho^{(1)}(s) = -\frac{1}{2\pi i} \oint_{|z|=s_0} dz w(z) \Pi^{(1)}(z) , \quad (2.3)$$

which is valid for any $s_0 > 0$ and any weight $w(s)$ analytic inside and on the contour $|z| = s_0$ in the complex plane [49–57].⁶ We will choose $w(z)$ to be polynomial in z .

The basic idea for extracting α_s from hadronic τ decay data is then to evaluate the left-hand side of Eq. (2.3) using experimental data for the spectral function, while taking s_0 large enough that QCD perturbation theory provides a good representation of the right-hand side. As the value of s_0 for which spectral data is available is kinematically limited to $s_0 \leq m_\tau^2$, non-perturbative corrections to the right-hand side are potentially non-negligible, and we discuss our framework for including them below. When the need arises, we will refer to the $w(s)$ -weighted spectral integral above as $I_{\text{ex}}^{(w)}(s_0)$, and the corresponding weighted $|z| = s_0$ contour integral as $I_{\text{th}}^{(w)}(s_0)$.

For large enough $|s| = s_0$, and sufficiently far away from the Minkowski axis $z = s > 0$, $\Pi(s)$ can be approximated by the OPE

$$\Pi_{\text{OPE}}(z) = \sum_{k=0}^{\infty} \frac{C_{2k}(z)}{(-z)^k} , \quad (2.4)$$

where the logarithmic z dependence of the OPE coefficients C_{2k} can in principle be calculated in perturbation theory.

⁶ If one retains the up-down quark mass difference, the two-point function also depends on a scalar, spin-0 polarization, whose spectral function is $O((m_d - m_u)^2)$, and which is safely negligible given the precision of current isovector V spectral data. With spin 0 contributions negligible, we will drop the superscripts (1) in what follows and denote $\Pi^{(1)}$ by Π and $\rho^{(1)}$ by either ρ or $\rho_{ud;V}$.

For the $k = 0$ term, one usually considers, instead of $\Pi(z)$, the Adler function $D(z) \equiv -z d\Pi(z)/dz$, which is finite and formally independent of the renormalization scale μ . Accordingly, the $k = 0$ contribution to the right-hand side of Eq. (2.3) can be expressed in terms of the corresponding contribution to the Adler function via partial integration. The dimension $D = 0$ contribution $D_0(z)$ to $D(z)$ takes the form

$$D_0(z) \equiv -z \frac{dC_0(z)}{dz} = \frac{1}{4\pi^2} \sum_{n=0}^{\infty} \left(\frac{\alpha_s(\mu^2)}{\pi} \right)^n \sum_{m=1}^{n+1} m c_{nm} \left(\log \frac{-z}{\mu^2} \right)^{m-1}, \quad (2.5)$$

where the coefficients c_{nm} are known to order α_s^4 [32]. In the $\overline{\text{MS}}$ scheme, $c_{01} = c_{11} = 1$, $c_{21} = 1.63982$, $c_{31} = 6.37101$ and $c_{41} = 49.07570$, for three flavors [32]; all other coefficients to this order can be determined using the scale independence of $D_0(z)$ and the renormalization group. While c_{51} is not known at present, we will use the estimate $c_{51} = 283 \pm 142$, which generously covers all estimates for this coefficient that can be found in the literature [32, 58–60]. For the running of α_s we use the four-loop $\overline{\text{MS}}$ β -function, but we have checked that using five-loop running instead [61, 62] leads to differences of order 10^{-4} or less in our results for $\alpha_s(m_\tau^2)$. As already mentioned in the introduction, for evaluating the perturbative contribution to the FESR (2.3) we will choose $\mu^2 = s_0$ in Eq. (2.5), which corresponds to using FOPT.

The C_{2k} contain non-perturbative $D = 2k$ condensate contributions for $k > 1$. As in Ref. [9], we will neglect purely perturbative quark-mass contributions to C_{2k} , $k \geq 1$, as they are numerically very small for the non-strange V channel FERSs considered in this paper. We will also neglect the z -dependence of the coefficients C_{2k} for $k > 1$.⁷ It then follows that, for weights $w(y)$ polynomial in $y = s/s_0$, $D = 2k > 2$ contributions to the contour integral $I_{\text{th}}^{(w)}(s_0)$ are proportional to C_{2k}/s_0^k , and present only if $w(y)$ contains a term proportional to y^{k-1} . A more detailed discussion of our treatment of the $D > 0$ OPE contributions, including a response to Ref. [34], may be found in Refs. [37, 46].

So far, our strategy is based on standard OPE-based QCD tools. However, the OPE breaks down near the Minkowski axis [63]. If the OPE would also hold for $z = s > 0$, Eq. (2.3) would establish a direct correspondence between the OPE and the resonant behavior of the experimental spectral function, generally referred to as quark-hadron duality. However, it is clear that the OPE cannot account for the oscillatory resonance behavior of the spectral function seen up to fairly large values of s , and thus quark-hadron duality is violated. We briefly review our approach to this problem, as this is where our strategy differs from others used in the literature.

We account for the breakdown of this duality by replacing the right-hand side of Eq. (2.3) by

$$-\frac{1}{2\pi i s_0} \oint_{|z|=s_0} dz w(z) (\Pi_{\text{OPE}}(z) + \Delta(z)), \quad (2.6)$$

with

$$\Delta(z) \equiv \Pi(z) - \Pi_{\text{OPE}}(z), \quad (2.7)$$

defining the quark-hadron duality violating contribution $\Delta(z)$ to $\Pi(z)$. One expects $\Delta(z)$ to decay exponentially for $|z| \rightarrow \infty$, and thus for polynomial weights Eq. (2.6) can be rewritten

⁷ Such logarithmic corrections, which are suppressed by additional powers of α_s , are known only for low values of k .

as [64]

$$I_{\text{th}}^{(w)}(s_0) = -\frac{1}{2\pi i s_0} \oint_{|s|=s_0} dz w(z) \Pi_{\text{OPE}}(z) - \frac{1}{s_0} \int_{s_0}^{\infty} ds w(s) \frac{1}{\pi} \text{Im} \Delta(s) . \quad (2.8)$$

The imaginary part $\frac{1}{\pi} \text{Im} \Delta(s)$ can be interpreted as the duality-violating part $\rho^{\text{DV}}(s)$ of the non-strange V spectral function, and represents the resonance-induced, oscillatory parts of the spectral function not captured by the OPE.

In Ref. [65], we developed a theoretical framework for quark-hadron duality violations in terms of a generalized Borel–Laplace transform of $\Pi(q^2)$ and hyperasymptotics, building on earlier work [66–69]. In the chiral limit, and assuming the spectrum becomes Regge-like asymptotically at large s in the $N_c \rightarrow \infty$ limit, we showed that the large- s form of $\rho^{\text{DV}}(s)$ can be parametrized as

$$\rho^{\text{DV}}(s) = \frac{1}{\pi} \text{Im} \Delta(s) = \left(1 + \frac{c}{s}\right) e^{-\delta - \gamma s} \sin(\alpha + \beta s) , \quad (2.9)$$

up to slowly varying logarithmic corrections and with $\gamma \sim 1/N_c$ small but non-zero.⁸ The parameter β is directly related to the Regge slope, and the parameter γ to the (asymptotic) ratio of the width and mass of the resonances. The DV parameters are to be fitted along with $\alpha_s(m_\tau^2)$ and the other OPE parameters to the weighted spectral integrals of Eq. (2.3). In Eq. (2.9), we have allowed for a multiplicative correction of order $1/s$ [65], the effect of which will be quantitatively investigated in Sec. IV C. While the framework of Ref. [65] is rather general and based on generally accepted conjectures about QCD (primarily Regge-like behavior), Ref. [65] does not provide a first-principle derivation from QCD. This introduces model dependence into our analysis which, however, can be tested by fits to the data. Such tests, in particular, will provide information about the values of s above which this asymptotic form is likely to be sufficiently accurate. We emphasize that modifications to the parametrization of Eq. (2.9) are constrained by the general framework of Ref. [65]. For a more recent discussion of our framework we refer to Ref. [37], which also addresses recent criticism leveled against our strategy in Ref. [34].

In summary, as in Refs. [9, 46–48], we will assume that Eq. (2.9) holds for $s \geq s_{\text{min}}$, with s_{min} to be determined from fits to the data. This assumes of course that the s_{min} for which this assumption is valid includes a region below m_τ^2 , *i.e.*, that both the OPE (2.4) and the DV parametrization (2.9) can be used in some interval below m_τ^2 .

B. Choice of weight functions and the OPE

The logarithmic s dependence of the OPE coefficients $C_D(s)$ is calculable in perturbation theory; this s dependence is an $\mathcal{O}(\alpha_s^2)$ effect in the chiral limit. Such effects were found to be safely negligible for $D = 4$ and $D = 6$ in the sum-rule analysis of the OPAL data reported in Ref. [46], and again in Ref. [37], and we will thus ignore them for $D > 0$ in the present analysis as well.⁹ This assumption is common to all α_s analyses using τ -decay data. As noted above, assuming the coefficients $C_D(z)$ to be z independent, a term proportional to the monomial z^n in the (polynomial) weight $w(z)$ projects onto the $D = 2(n + 1)$ OPE

⁸ This form (without the c/s correction) was first introduced in Ref. [70], and subsequently used in Refs. [46–48, 64, 71].

⁹ Nothing is known about logarithmic corrections beyond $D = 6$.

contribution in the sum rule (2.3).¹⁰ If $w(z)$ has degree k , the right-hand side of (2.3) then contains only a finite number of $D > 0$ OPE contributions, having maximum dimension $D = 2k + 2$.

In this paper, we will consider the weights $w(z) = w_n(z/s_0)$ with

$$\begin{aligned} w_0(y) &= 1, \\ w_2(y) &= 1 - y^2, \\ w_3(y) &= (1 - y)^2(1 + 2y), \\ w_4(y) &= (1 - y^2)^2, \end{aligned} \tag{2.10}$$

where the subscript indicates the degree of the polynomial. These weights explore OPE terms with $D \leq 10$, and form a linearly independent basis for polynomials up to degree four without a linear term. The weight $w_0(y)$ projects only the $D = 0$ term of the OPE (*i.e.*, pure perturbation theory), while the weight $w_2(y)$ projects onto $D = 0$ and $D = 6$, the weight $w_3(y)$ onto $D = 0$, $D = 6$ and $D = 8$, and the weight $w_4(y)$ onto $D = 0$, $D = 6$ and $D = 10$. As the OPE is at best an asymptotic expansion in $1/z$, it is safer to limit oneself to sum rules with low-degree weights such as $w_0(y)$ and $w_2(y)$, and check for consistency among sum rules with different, higher-degree weights. As explained in Ref. [46], we choose to avoid weights with a linear term in y , as renormalon-based studies suggest that such weights are perturbatively unstable [58, 72–74].

The different sensitivity of these weights to DVs also allows us to have some control on the possible systematic error coming from the approximate nature of the DV parametrization (2.9). The weights $w_{2,3,4}(y)$ are “pinched,” *i.e.*, they have zeros at $z = s_0$, and thus suppress contributions from the region near the timelike point $z = s_0$ on the contour and hence also DV contributions to the associated FESRs [75, 76]. The weight $w_2(y)$ has a single zero at $z = s_0$ (a single pinch), while the weights $w_3(y)$ and $w_4(y)$ are doubly pinched, *i.e.*, have a double zero at $z = s_0$.¹¹ In order to maintain maximal sensitivity to the DV parameters δ , γ , α and β , we will always include the $w_0(y)$ FESR in our fits. For a more detailed discussion of this aspect of our strategy, we refer to Sec. IV A.

III. DATA

In this section, we will describe in detail our procedure for combining the ALEPH, OPAL and Belle $\pi^-\pi^0$ data and ALEPH and OPAL $2\pi^-\pi^+\pi^0$ and $\pi^-3\pi^0$ data. We begin by detailing the sources of all the data used in this paper in Sec. III A, after which, in Sec. III B, we describe our data-combination algorithm. We then present the $\pi^-\pi^0$ combination in Sec. III C and the two-mode 4π combination of ALEPH and OPAL $2\pi^-\pi^+\pi^0$ and $\pi^-3\pi^0$ data in Sec. III D. In Sec. III E the resulting 2π and 4π contributions are added together, using suitable interpolation and taking into account correlations between the 2π and 4π contributions introduced by the BF correlations. Finally, in Sec. III F, we add the residual mode contributions from Ref. [9] to arrive at our new result for the inclusive non-strange V spectral function, $\rho(s)$. In what follows, we will denote the contribution of a given exclusive mode, or exclusive-mode combination, X , to $\rho(s)$ as $\rho_X(s)$, and refer to this quantity as “the mode- X spectral function.” As explained in Sec. I, we do not include the CLEO data

¹⁰ The $D = 0$ term, perturbation theory, of course contributes for all n .

¹¹ The oscillatory dependence of $\rho^{\text{DV}}(s)$ on s , of course, produces an oscillatory dependence of weighted DV integrals on s_0 . Employing FESRs with multiple s_0 thus provides implicit tests of the assumed DV form.

for the $\pi^-\pi^0$ mode in the construction of the inclusive spectral function. Instead, we discuss the impact of including the CLEO data in App. B, where it is shown that the impact is small.

A. External input

ALEPH exclusive-mode $X = \pi^-\pi^0, 2\pi^-\pi^+\pi^0, \pi^-3\pi^0$ data are provided in the form of the BF-normalized experimental number distributions $\frac{B_X}{N_X} \frac{dN_X(s)}{ds}$. These are related to the corresponding mode- X spectral functions by [2]

$$\rho_X(s) = \frac{m_\tau^2}{12\pi^2 B_e S_{\text{EW}} |V_{ud}|^2 w_T^{\text{av}}(s; m_\tau^2)} \frac{B_X}{N_X} \frac{dN_X(s)}{ds} \quad (3.1)$$

with B_X the $\tau \rightarrow X\nu_\tau$ BF for exclusive mode X , B_e the $\tau \rightarrow e\nu_\tau\bar{\nu}_e$ BF, and $w_T^{\text{av}}(s; s_0)$ defined as [48]

$$w_T^{\text{av}}(s = \mathbf{sbin}(\mathbf{i}); m_\tau^2) = \frac{1}{\mathbf{dsbin}(\mathbf{i})} \int_{\mathbf{sbin}(\mathbf{i}) - \mathbf{dsbin}(\mathbf{i})/2}^{\mathbf{sbin}(\mathbf{i}) + \mathbf{dsbin}(\mathbf{i})/2} w_T(s; m_\tau^2) ds, \quad (3.2)$$

where $\mathbf{sbin}(\mathbf{i})$ is the i -th bin center, $\mathbf{dsbin}(\mathbf{i})$ is the i -th bin width, and $w_T(s; s_0)$ is the kinematic weight

$$w_T(s; s_0) \equiv w_3(s/s_0) = \left(1 - \frac{s}{s_0}\right)^2 \left(1 + 2\frac{s}{s_0}\right). \quad (3.3)$$

To perform the conversion (3.1) we require the hadronic BFs B_X , together with input for the external parameters, B_e , the short-distance electroweak correction factor S_{EW} , the ud Cabibbo–Kobayashi–Maskawa matrix element $|V_{ud}|$ and the τ mass m_τ . The external parameters appear in the fixed combination

$$\mathcal{F} = \frac{12\pi^2 B_e S_{\text{EW}} |V_{ud}|^2}{m_\tau^2}. \quad (3.4)$$

We employ for the BFs B_X and correlations between them the HFLAV 2022 Ref. [30] results¹²

$$\begin{aligned} B_{2\pi} &\equiv B_{\pi^-\pi^0} = 0.25486(90), \\ B_{1\pi^0} &\equiv B_{2\pi^-\pi^+\pi^0} = 0.04480(55), \\ B_{3\pi^0} &\equiv B_{\pi^-3\pi^0} = 0.01040(71), \\ r_{\pi^-\pi^0, 2\pi^-\pi^+\pi^0} &= -0.13, \\ r_{2\pi^-\pi^+\pi^0, \pi^-3\pi^0} &= -0.01, \\ r_{\pi^-\pi^0, \pi^-3\pi^0} &= +0.01, \end{aligned} \quad (3.5)$$

where $r_{X,Y}$ is the correlation between B_X and B_Y . Note that the 2022 HFLAV updates differ from the then-current, HFLAV 2019 Ref. [28] inputs used in Ref. [9]. Of particular numerical significance are the 9% downward shift in central value and factor of 2.4 increase

¹² The BFs and errors in Eqs. (3.5) are unchanged in the even more recent HFLAV 2024 update [77]. HFLAV 2022, however, quotes the BFs and errors to one more significant figure than does HFLAV 2024 and has the additional advantage of listing the basis-mode BF correlations, which are not tabulated in HFLAV 2024.

in error relative to HFLAV 2019 seen in the HFLAV 2022 $B_{\pi-3\pi^0}$ result. The values used for the external parameters (omitting the errors on m_τ , $|V_{ud}|$, and S_{EW} , for which the relative errors are much smaller than that on B_e) are (from, respectively, Ref. [1] for m_τ and $|V_{ud}|$, Ref. [30] for B_e and Ref. [78] for S_{EW})

$$\begin{aligned} m_\tau &= 1.77693 \text{ GeV} , \\ |V_{ud}| &= 0.97367 , \\ B_e &= 0.17812(22) , \\ S_{EW} &= 1.0201 , \end{aligned} \tag{3.6}$$

and lead to

$$\mathcal{F} = 6.4613(80) \text{ GeV}^{-2} . \tag{3.7}$$

The conversion relation Eq. (3.1) and inputs above are, of course, also used to convert the covariances of the ALEPH BF-normalized number-distributions to those of $\rho_X(s)$.

OPAL quotes results in the form of the exclusive-mode contributions $\rho_X(s)$. These were obtained from the experimentally measured normalized number distributions via Eq. (3.1), using then-current values of the exclusive-mode BFs, B_X , and external inputs B_e , S_{EW} , $|V_{ud}|$ and m_τ . We have updated the OPAL $\rho_X(s)$ results, following Ref. [47], by first reconstructing the underlying unit-normalized distributions using the values for the exclusive-mode BFs and external inputs quoted by OPAL, and then converting back to $\rho_X(s)$ using the updated versions of these inputs quoted above.

Contrary to OPAL and ALEPH, Belle already provides the unit-normalized number distribution, $(1/N_X)dN_X/ds$, which produces the Belle version of $\rho_{2\pi}(s)$ after dividing by the relevant external factors and the averaged kinematic weight $w_T^{\text{av}}(s; m_\tau^2)$ and multiplying by $B_{2\pi}$. Again, the Belle data covariance matrices are scaled accordingly.

B. Data combination algorithm

Before getting to specific exclusive modes, we describe the underlying data combination algorithm, which goes back to Ref. [79], and has been used by Keshavarzi, Nomura and Teubner [29] to combine the world's electroproduction data in their determination of the hadronic contribution to the inclusive electromagnetic spectral function. We start by repeating the description of this algorithm given in Ref. [9], after which we discuss the generalization of the algorithm to include also non- χ^2 fit qualities.

Suppose we wish to combine the spectral data for a particular exclusive mode from a number of experiments. We begin with choosing a number of clusters, distributed over the interval $0 < s \leq m_\tau^2$, assigning a number of consecutive data points from all experiments to each cluster m , $m = 1, \dots, N_{\text{cl}}$, with N_{cl} the total number of clusters. n_m will be the total number of data points in cluster m . Parametrizing the data by pairs (s_i, d_i) , with d_i the data point for the spectral function assigned to the s -value s_i , we define weighted cluster averages

$$s^{(m)} = \sum_{i \in m} \frac{s_i}{\sigma_i^2} / \sum_{i \in m} \frac{1}{\sigma_i^2} , \tag{3.8}$$

where the sum is over all data points in cluster m and σ_i^2 is the variance of d_i , *i.e.*, the σ_i^2 are the diagonal elements of the covariance matrix C_{ij} for the spectral-function data points

d_i . The set of $s^{(m)}$ then constitutes the values of s at which the combined spectral function $\rho^{(m)}$ will be defined.

The values of $\rho^{(m)}$ are determined by a linear fit, minimizing

$$\chi^2(\rho) = \sum_{i=1}^N \sum_{j=1}^N (d_i - R(s_i; \rho)) C_{ij}^{-1} (d_j - R(s_j; \rho)) , \quad (3.9)$$

where $N = \sum_{m=1}^{N_{\text{cl}}} n_m$ is the total number of data points, and the piece-wise linear function $R(s; \rho)$ is defined by

$$R(s; \rho) = \rho^{(m)} + \frac{s - s^{(m)}}{s^{(m+1)} - s^{(m)}} \left(\rho^{(m+1)} - \rho^{(m)} \right) , \quad s^{(m)} \leq s \leq s^{(m+1)} , \quad 1 \leq m < N_{\text{cl}} , \quad (3.10)$$

where ρ is the vector of fit parameters $\rho^{(m)}$, $m = 1, \dots, N_{\text{cl}}$. At the boundaries, we extrapolate:

$$\begin{aligned} R(s; \rho) &= \rho^{(N_{\text{cl}}-1)} + \frac{s - s^{(N_{\text{cl}}-1)}}{s^{(N_{\text{cl}})} - s^{(N_{\text{cl}}-1)}} \left(\rho^{(N_{\text{cl}})} - \rho^{(N_{\text{cl}}-1)} \right) , \quad s \geq s^{(N_{\text{cl}})} , \quad (3.11) \\ R(s; \rho) &= \rho^{(1)} + \frac{s - s^{(1)}}{s^{(2)} - s^{(1)}} \left(\rho^{(2)} - \rho^{(1)} \right) , \quad s \leq s^{(1)} . \end{aligned}$$

Writing R as a rectangular matrix R_{im} such that

$$\sum_{m=1}^{N_{\text{cl}}} R_{im} \rho^{(m)} = R(s_i; \rho) \quad (3.12)$$

and using vector notation, the minimum of Eq. (3.9) is obtained at

$$\begin{aligned} \vec{\rho} &= M \vec{d} , \quad (3.13) \\ M &= (R^T C^{-1} R)^{-1} (R^T C^{-1}) , \end{aligned}$$

while the covariance matrix, \mathcal{C}_{mn} , of the cluster $\vec{\rho}$ parameters, is given by

$$\mathcal{C} = M C M^T . \quad (3.14)$$

Using Eq. (3.13), this reduces to

$$\mathcal{C}^{-1} = R^T C^{-1} R . \quad (3.15)$$

Note that the length of the parameter vector $\vec{\rho}$ is smaller than that of the data vector \vec{d} .

The algorithm described above applies if the full data covariance matrix is available and positive definite (and thus invertible). In our application to the data, this is always the case for the 2π data combination; the $\pi^- \pi^0$ ALEPH, OPAL and Belle covariance matrices are all positive definite, and the corresponding correlation matrices do not appear to have ‘‘suspiciously’’ small eigenvalues. However, this is not the case for the two 4π modes (as already observed in Ref. [9]), and this leads us to consider the minimization of a fit quality

$$Q^2 = (\vec{d} - R\vec{\rho})^T W^2 (\vec{d} - R\vec{\rho}) , \quad (3.16)$$

with the positive definite matrix W^2 replacing C^{-1} in Eq. (3.9). In such cases we use the methods of Ref. [80] to obtain the parameter covariance matrix \mathcal{C} and compute a p -value for the fit. In this case, one finds

$$M = (R^T W^2 R)^{-1} (R^T W^2) , \quad (3.17)$$

while \mathcal{C} is still obtained from Eq. (3.14) with M now given by Eq. (3.17). Of course, for $W^2 = C^{-1}$, one recovers Eqs. (3.9) and (3.15).

As in Ref. [9], in order to assess the local quality of our fits, we also, for each fit, compute the χ^2 (or Q^2) value and corresponding p -value for each cluster in the fit, *i.e.*, Eq. (3.9) restricted to each of the clusters labeled by m for all $m = 1, \dots, N_{\text{cl}}$, to check that there are no large local discrepancies between the different data sets. Such local χ^2 (or Q^2) computations will always use the full corresponding block-diagonal data covariance matrices, where the blocks are defined by the clusters.¹³ Note however, that in the case of a fully correlated global fit, the full χ^2 (3.9) is not equal to the sum of the local χ^2 values, as in general there will be non-vanishing correlations between data in different clusters.

For the 2π combination, described in Sec. III C below, we will combine the ALEPH, OPAL and Belle unit-normalized data, divided by $w_T(s; m_\tau^2)$, before multiplying with the factor $B_{\pi^-\pi^0}/\mathcal{F}$ required to produce the 2π spectral function. In the case of the 4π combination described in Sec. III D, however, we will need to first form the ALEPH and OPAL versions of the sum of $2\pi^-\pi^+\pi^0$ and $\pi^-3\pi^0$ spectral functions, including the factors $B_{2\pi^-\pi^+\pi^0}/\mathcal{F}$ and $B_{\pi^-3\pi^0}/\mathcal{F}$ in the process, before combining the ALEPH and OPAL results. In this case, the errors on the two BFs lead to a potential bias, known as the d'Agostini bias Ref. [45]. We will explain how this issue is handled in Sec. III D below.

C. ALEPH, OPAL and Belle 2π data combination

For the $\pi^-\pi^0$ exclusive mode, the ALEPH [4], OPAL [5] and Belle [6] unit-normalized number distribution data sets have positive definite covariance matrices, which allows us to combine them using the standard χ^2 fit analysis, described in Sec. III B. There are two advantages to performing the combination of the unit-normalized distributions first, rather than directly combining the three 2π spectral functions. First, this ensures the combination is not subject to a d'Agostini bias [45], which could arise from the correlations induced by the overall normalization with the BF. Second, since no BF needs to be included in the data before performing the combination, the effect of future changes in $B_{\pi^-\pi^0}$ can be incorporated by a global rescaling, without having to re-run the entire combination procedure.

An essential step in the combination method described in Sec. III B is choosing a reasonable strategy for dividing the data into clusters. Since the Belle data set is considerably more precise than those of ALEPH and OPAL, a first requirement we impose is that each cluster contain at least one Belle data point. Due to the rapid variation of the spectral function around the ρ peak, a finer grid of clusters is needed in this region, while clusters with more data points are used in the higher- s region where the data are sparser, more slowly varying, and have larger errors. With this strategy, from a comparison of the experimental uncertainties of the three data sets, we expect Belle to dominate the combination.

¹³ In the case of the $\pi^-3\pi^0$ mode, only the diagonal part of the OPAL covariance matrix is used, see Sec. III D below.

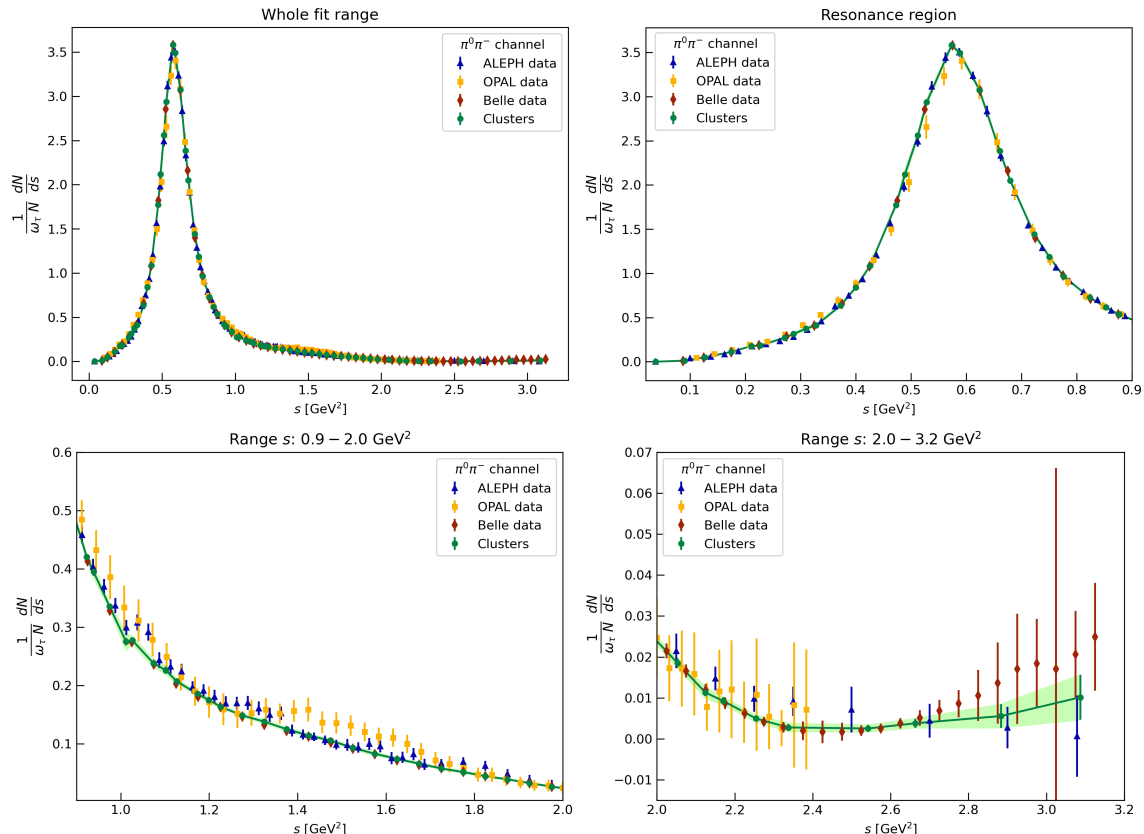


FIG. 1. Results of the fit for the 63-cluster combination of the $\pi^- \pi^0$ exclusive-mode unit-normalized distribution divided by the s -dependent kinematic weight factor. The error bars represent the uninflated errors, while inflated errors are represented by the green band.

Our combined 2π results are obtained from a configuration with 63 clusters, which produces a global fit quality of

$$\chi^2/\text{dof} = 168.65/150, \quad p\text{-value} = 14\%. \quad (3.18)$$

The results of this combined fit are shown by the green points in Fig. 1, together with the corresponding single-experiment ALEPH, OPAL and Belle inputs. We have considered alternate choices of clusters following the same principles, and always obtained very similar results.

We have also computed local χ_{cl}^2 values, *i.e.*, χ^2 values for each cluster, from our fit results. The goal of the local χ_{cl}^2 calculation is to check whether the three different data sets agree also locally, in each cluster. With the number of degree of freedom in each cluster known, we can convert the local χ_{cl}^2 values into local p_{cl} -values, which are shown in Fig. 2.¹⁴ The p_{cl} -values of the clusters are generally good, with the exception of three clusters for which $p_{\text{cl}} \sim 0.005$. We conclude that the three data sets are statistically compatible. For clusters with a local χ_{cl}^2 values larger than 1, we account for the tension between the data sets in

¹⁴ There are three clusters with only one data point, *i.e.*, with no degrees of freedom. For such clusters, we set the p_{cl} -value equal to 1.

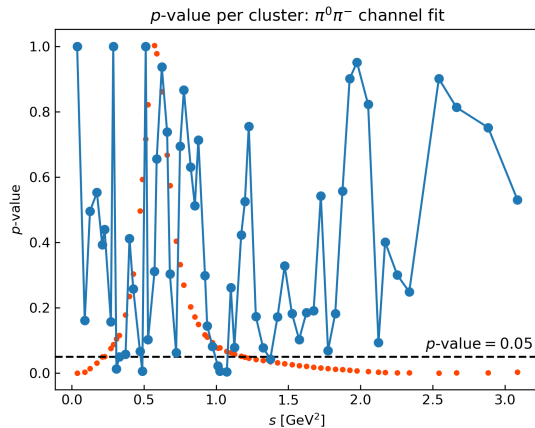


FIG. 2. Local p -value for each cluster, for the 63-cluster $\pi^-\pi^0$ unit-normalized combined spectral function. The red dots show, up to an arbitrary overall normalization, the corresponding combined 2π spectral function.

each such cluster by inflating the errors, multiplying them by $\sqrt{\chi_{\text{cl}}^2}$. The resulting inflated errors are shown by the green bands in Fig. 1. No error rescaling is performed for clusters with local χ^2 values smaller than 1. As can be seen in Fig. 1, the difference between the error bars on the green points and the green band is barely visible.

Figure 3 shows the ratio of each of the three single-experiment 2π spectral functions to the combined version, in the region around the ρ peak. The impact of the Belle data is obvious: they dominate the final combined spectrum, especially in the ρ -peak region. While the quality of the fit is good, it can be seen that in the region just beyond the ρ peak, the Belle data lie systematically somewhat below the combined $\pi^-\pi^0$ distribution. Figure 3 can be compared to similar figures in Ref. [4].

D. ALEPH and OPAL 4π data combination

In order to prepare the ALEPH [4] and OPAL [5] data sets, we discard the small number of $2\pi^-\pi^+\pi^0$ and $\pi^-3\pi^0$ points having total or systematic error equal to zero, assuming such points cannot be interpreted as reliably determined data.

Unlike the case of the 2π data, the unit-normalized $2\pi^-\pi^+\pi^0$ and $\pi^-3\pi^0$ covariance matrices of ALEPH and OPAL are ill-behaved. The ALEPH $2\pi^-\pi^+\pi^0$ and $\pi^-3\pi^0$ correlation matrices have 1 and 14 negative eigenvalues of order 10^{-9} and 10^{-6} or less in magnitude, respectively, while the OPAL $\pi^-3\pi^0$ covariance matrix has 1 negative eigenvalue with magnitude of order 10^{-2} .

Because of these issues with the exclusive-mode 4π covariance matrices, combining their unit-normalized number distributions following the same procedure as employed for the $\pi^-\pi^0$ case (using fully correlated fits) is not possible. However, summing the $\pi^-3\pi^0$ and $2\pi^-\pi^+\pi^0$ contributions (properly normalized with the corresponding BFs) to produce the total 4π spectral function for each of ALEPH and OPAL, we find that both of the associated

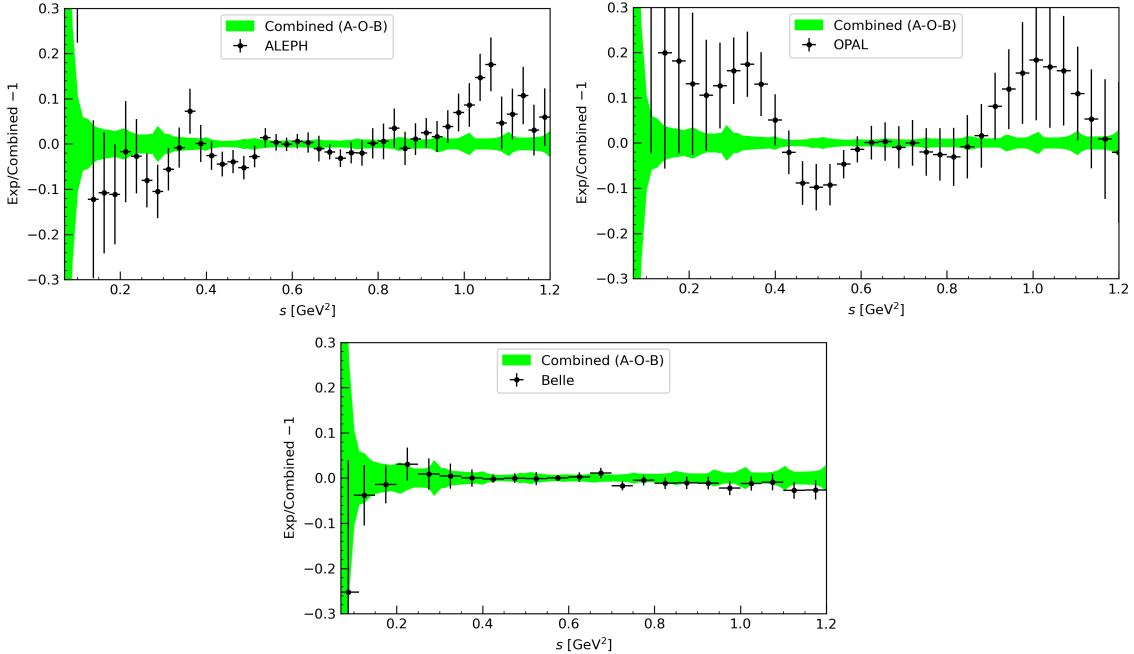


FIG. 3. Ratio between experimental 2π data and the associated 2π combination, in the ρ peak region.

total 4π covariance matrices are positive definite. The total 4π covariance matrix for OPAL, however, has very small (positive) eigenvalues indicating very strong correlations, and a standard χ^2 fit employing Eq. (3.9) leads to a global ALEPH plus OPAL combination with a p -value less than 0.1%.

We show the four exclusive-mode 4π data correlation matrices in Fig. 4. As is immediately evident, the qualitative pattern is very different in the OPAL $\pi^-3\pi^0$ case. It is this $\pi^-3\pi^0$ covariance matrix that leads to the poor combined fit.¹⁵

We thus depart from a strict χ^2 fit and turn to a fit using Eq. (3.16) with the ALEPH and OPAL exclusive-mode 4π spectral functions as input. The W^2 matrix used in Eq. (3.16) is constructed as follows. We replace the OPAL $\pi^-3\pi^0$ covariance matrix with a diagonal truncation, thus removing the strong, but poorly determined, correlations. The matrix W^2 of Eq. (3.16) is then constructed from the unmodified ALEPH $2\pi^-\pi^+\pi^0$ and $\pi^-3\pi^0$ covariance matrices, the unmodified OPAL $2\pi^-\pi^+\pi^0$ covariance matrix, and the diagonally truncated OPAL $\pi^-3\pi^0$ covariance matrix. As already mentioned, we keep the full, original data covariance matrices for error propagation, *i.e.*, the $\vec{\rho}$ parameter covariance matrix \mathcal{C} is computed with the full data covariance matrix C , using Eq. (3.14) with M as given in Eq. (3.17).

Since the $2\pi^-\pi^+\pi^0$ and $\pi^-3\pi^0$ spectral functions which serve as inputs to the fit have global normalizations set by the corresponding exclusive-mode BFs, our fit procedure po-

¹⁵ This poor behavior is most likely due to the difficulty of identifying neutral pions experimentally, leading to strong correlations with the $\pi^-\pi^0$ and $\pi^-2\pi^0$ exclusive-mode results. We thank Sven Menke for a detailed discussion of this point and the underlying experimental issues.

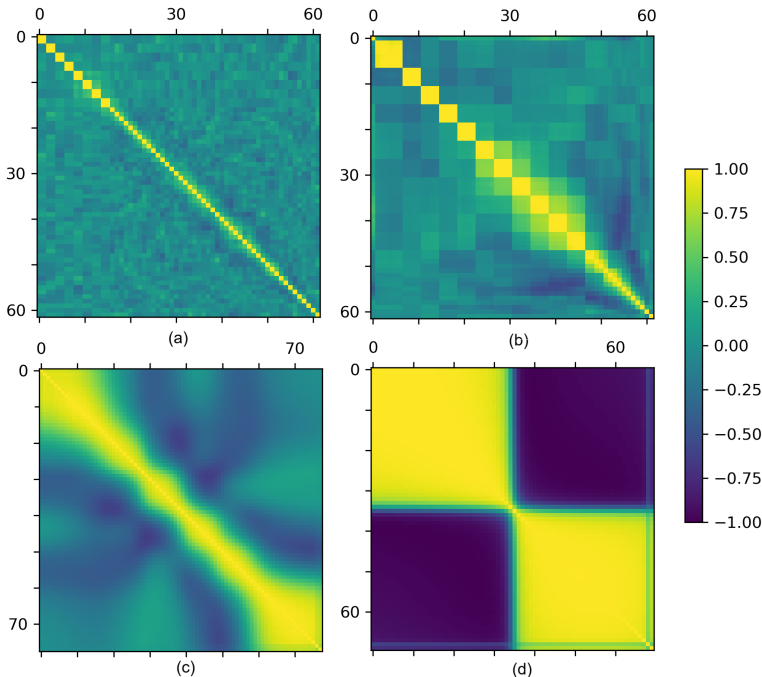


FIG. 4. Correlations of the unit-normalized, 4π exclusive-mode number distribution data sets. (a) ALEPH $2\pi^-\pi^+\pi^0$, (b) ALEPH $\pi^-3\pi^0$, (c) OPAL $2\pi^-\pi^+\pi^0$ and (d) OPAL $\pi^-3\pi^0$.

tentially suffers from the d’Agostini bias. In principle, one would like to use the iterative procedure proposed in Ref. [79] in order to correct for this bias, but, since after the first iteration only the sum of the two exclusive-mode 4π contributions is available, we have to resort to an approximate method, which is described in App. A. Our results presented below have been obtained using this approximate bias-correction method. The fact that the correction shifts the uncorrected result by only a small amount gives us confidence that the bias is not a significant effect.

Our result for the ALEPH plus OPAL two-mode 4π spectral function combination has 46 clusters, and a global fit quality of

$$p\text{-value} = 10.3\% , \quad (3.19)$$

computed following the procedure described in Ref. [80]. The resulting 4π combination is shown in Fig. 5, and the local p_{cl} -values, calculated using the methods of Ref. [80], in Fig. 6. As in the case of the 2π fit, there are no clusters with unacceptably small local p_{cl} -values (with none having a p_{cl} -value < 0.01). As before, green bands in the figure show inflated error bars computed as in Sec. III C; differences with the uninflated errors represented by the green error bars are barely visible.

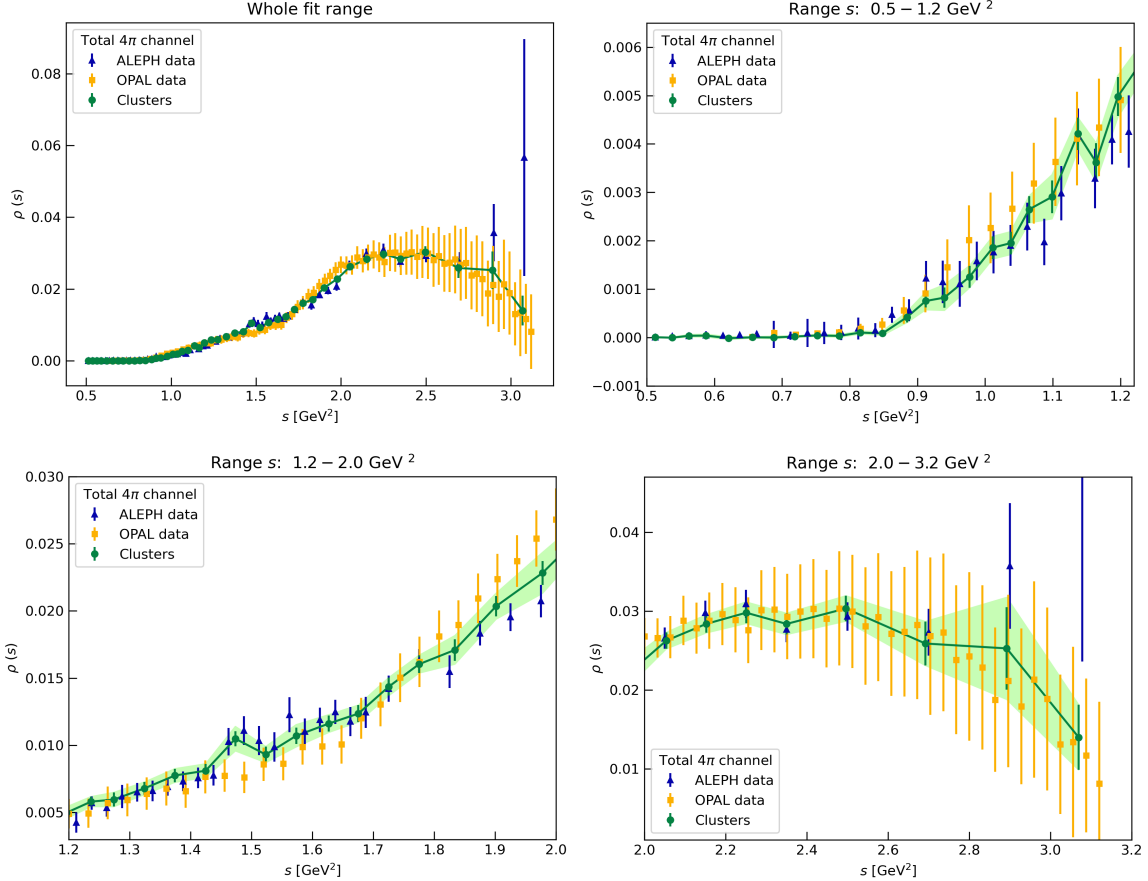


FIG. 5. Results (green points) of the fit for the 46-cluster combination of the ALEPH and OPAL two-mode 4π spectral function results. The error bars on the green points represent the uninflated errors, while inflated errors are represented by the green band.

E. Full 2π and 4π data combination

In this section, we outline how we combine the $\pi^-\pi^0$ spectral function obtained in Sec. III C with the total 4π spectral function obtained in Sec. III D. This would be trivial if there were no correlations between the 2π and 4π results: one would simply construct the combined 2π spectral function from the chosen input external constants and unit-normalized 2π result of Sec. III C, interpolate the 4π spectral function of Sec. III D to the s values of the 2π spectral-function clusters, and add the two results.

There are, however, two sources of correlation between the 2π and 4π spectral functions. First, there are the correlations inherent to the ALEPH and OPAL experiments themselves; see, for instance, the discussion of the OPAL $\pi^-3\pi^0$ covariance matrix in Sec. III D. These correlations have not been provided by the experiments, and we thus have to assume that they are relatively small.¹⁶ Second, there are correlations induced by the correlations

¹⁶ This assumption, though not made explicit, was also made in Ref. [9].

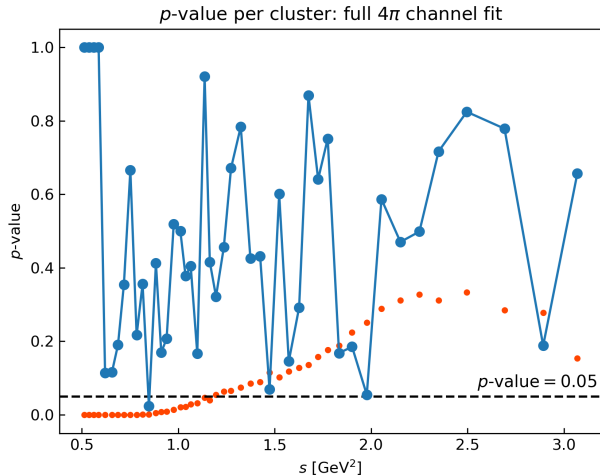


FIG. 6. Local p -value for each cluster, for the 46-cluster 4π spectral function combination. The red dots show, up to an arbitrary overall normalization, the corresponding combined 4π spectral function.

between the different exclusive-mode BFs, *cf.* the r -values given in Eq. (3.5). These correlations are also quite small, but since they have been provided by HFLAV [30], there is no reason not to take them into account.

Appendix C provides a detailed description of our procedure for including them and generating the $2\pi + 4\pi$ spectral function, $\rho_{2\pi+4\pi}(s)$, and associated covariance matrix. If information on other sources of correlation between the 2π and 4π data were to become available, those correlations can be taken into account following the same strategy.

With the $2\pi + 4\pi$ combination complete, the last step remaining in the construction of the inclusive spectral function is the addition of residual-mode contributions. This step is discussed in Sec. III F.

F. The inclusive non-strange V spectral function

With the $2\pi + 4\pi$ spectral function, generated using the algorithm described in App. C, in hand, the next step is to add the remaining, residual-mode contributions to produce the total inclusive spectral function. In the original ALEPH and OPAL publications, lacking reliable experimental determinations, Monte-Carlo input was used in obtaining the contributions from these modes. Our approach to these contributions was already discussed in Ref. [9], and details of how the exclusive residual-mode contributions were obtained from (i) 2019 BaBar $\tau \rightarrow K\bar{K}\nu_\tau$ data, and (ii) exclusive-mode $e^+e^- \rightarrow$ hadrons cross-sections using CVC, can be found in Ref. [9]. Since the work of Ref. [9], there have been no significant changes in the relevant experimental branching fractions, and no new data sets that would impact our previous work. We thus employ for the residual-mode contributions the results of Ref. [9], re-interpolated onto the grid of s values of the new 63-cluster set.

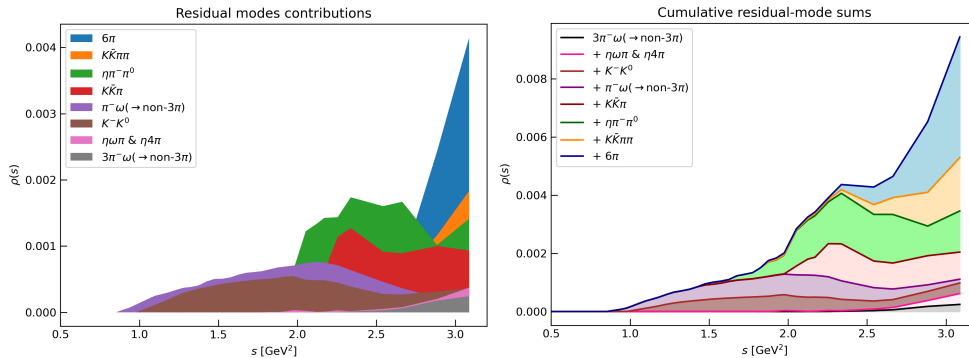


FIG. 7. *Residual-mode contributions to the inclusive spectral function. The left panel shows individual residual-mode contributions, the right panel the corresponding cumulative residual-mode totals.*

The residual modes for which spectral function contributions can be obtained, using CVC, from exclusive-mode electroproduction cross-sections are $\pi^-\omega(\rightarrow \text{non-}3\pi)$ [11, 12], $\eta\pi^-\pi^0$ [13–18], $K\bar{K}\pi$ [19], 6π [20–25], $K\bar{K}\pi\pi$ [19], $(3\pi)^-\omega(\rightarrow \text{non-}3\pi)$ [20], $\pi^-\eta\omega(\rightarrow \text{non-}3\pi)$ [26] and $\eta4\pi$ [26, 27]. The remaining residual-mode contribution, that of K^-K^0 , is, as noted above, obtained directly from the τ decay results of Ref. [10]. The contribution of each residual mode to the residual-mode spectral function total is shown in Fig. 7. In order to add these contributions to the combined $2\pi + 4\pi$ -mode sum, we have linearly interpolated each residual mode data set to the central values $s^{(m)}$ of the 63 2π mode clusters. The residual-mode covariance matrices were interpolated accordingly.

The final result for the inclusive isovector V spectral function, $\rho_{ud;V}(s)$, is given by the sum of the $\rho_{2\pi+4\pi}$ contributions from Secs. III C, III D and III E and the interpolated residual-mode results. In the left panel of Fig. 8 we show the individual contributions (2π , 4π and residual mode total) to $\rho_{ud;V}(s)$, and in the right panel, the total inclusive spectral function (with the light-blue band representing the inflated errors). Numerical versions of these result, with both uninflated and inflated errors, are presented in Tab. 1. The accompanying covariance matrix is too large to be tabulated here, but can be requested from the authors.

IV. THE STRONG COUPLING

In this section, we employ our new inclusive, non-strange V spectral function to evaluate the spectral moments $I_{\text{exp}}^{(w)}(s_0)$ of Eq. (2.3), with the weights defined in Eq. (2.10), in order to determine $\alpha_s(m_\tau^2)$. Our analysis follows the same strategy as in Ref. [9]. We briefly comment on our strategy in Sec. IV A, and present our results in Sec. IV B. Section IV C provides further analysis and discussion.

s	$2\pi^2\rho_{ud;V}(s)$	s	$2\pi^2\rho_{ud;V}(s)$	s	$2\pi^2\rho_{ud;V}(s)$	s	$2\pi^2\rho_{ud;V}(s)$
0.038	0.000(00)(00)	0.529	2.286(20)(28)	1.026	0.258(05)(07)	1.725	0.353(13)(13)
0.090	0.009(02)(03)	0.574	2.790(16)(16)	1.073	0.245(05)(07)	1.775	0.383(13)(13)
0.126	0.038(02)(02)	0.588	2.720(19)(19)	1.102	0.243(08)(10)	1.825	0.399(15)(19)
0.175	0.086(03)(03)	0.624	2.395(15)(15)	1.126	0.245(06)(07)	1.875	0.441(14)(17)
0.211	0.138(05)(05)	0.661	1.857(17)(17)	1.173	0.233(07)(07)	1.925	0.478(14)(20)
0.227	0.142(04)(04)	0.680	1.597(12)(13)	1.199	0.246(08)(09)	1.975	0.509(17)(29)
0.271	0.212(05)(06)	0.723	1.123(08)(12)	1.226	0.249(07)(07)	2.053	0.589(21)(21)
0.288	0.244(09)(09)	0.750	0.925(10)(10)	1.275	0.247(10)(10)	2.125	0.621(20)(20)
0.310	0.291(07)(17)	0.777	0.751(07)(07)	1.325	0.256(09)(10)	2.170	0.640(22)(22)
0.329	0.322(05)(09)	0.824	0.566(05)(05)	1.375	0.266(10)(10)	2.254	0.668(27)(27)
0.373	0.496(06)(10)	0.853	0.482(08)(08)	1.425	0.266(10)(10)	2.337	0.652(25)(25)
0.400	0.654(09)(09)	0.877	0.424(04)(04)	1.475	0.308(11)(18)	2.542	0.664(32)(32)
0.426	0.846(06)(07)	0.923	0.344(04)(05)	1.525	0.277(12)(12)	2.664	0.618(50)(50)
0.473	1.380(10)(14)	0.938	0.325(07)(09)	1.575	0.297(12)(16)	2.884	0.632(102)(125)
0.489	1.649(17)(44)	0.975	0.288(05)(06)	1.625	0.308(12)(13)	3.087	0.448(93)(93)
0.513	1.994(23)(23)	1.012	0.255(07)(12)	1.675	0.319(12)(13)		

TABLE 1. Total inclusive spectral function multiplied by $2\pi^2$. The first and second errors are, respectively, the uninflated and inflated ones. For reference, the parton-model value for $2\pi^2\rho_{ud;V}(s)$ is $\frac{1}{2}$.

A. Strategy

In the first, and main step of our analysis, we use the spectral integrals, $I_{\text{exp}}^{(w_0)}(s_0)$, of the $w_0 = 1$ FESR to determine $\alpha_s(m_\tau^2)$ and the DV parameters δ , γ , α and β , considering all s_0 in the interval between a value s_0^{min} and the maximum value available for our 63-cluster spectral function. We vary s_0^{min} , and look for a region in which the fits (as measured by the p -values) are good, at the same time demanding stability of the results with respect to s_0^{min} . We then average $\alpha_s(m_\tau^2)$ over the fits in this stability region. While the spectral integrals for nearby values of s_0 are highly correlated, there is no problem with carrying out these fits: we find a “plateau” region of s_0^{min} values with stable, high-quality fits. The central value of our final result, as well as the statistical error, are obtained from these fits, taking into account the correlations between the results for different s_0^{min} .

In the second step, we perform combined fits using two different weights, one of which is always the weight w_0 , and the other is w_i , with $i = 2, 3, 4$. As the weights $w_{2,3,4}$ are pinched, the corresponding spectral integrals are less sensitive to the DV parameters, making it more difficult to reliably determine these parameters in fits that do not also include $I_{\text{exp}}^{(w_0)}(s_0)$. The motivation for performing such two-weight, multiple- s_0 fits is that the addition of the second-weight integrals produces new, non-trivial constraints on the associated theoretical representations.¹⁷

¹⁷ As an example, consider the step-two choice $w_2(y) = 1 - y^2$. The theory side of the new w_2 FESR introduces the single new fit parameter, C_6 . If the step-one theory representation is reliable, the difference between $I_{\text{ex}}^{(w_2)}$ and the sum of $D = 0$ and DV contributions to $I_{\text{th}}^{(w_2)}$ implied by the step-one α_s and DV-parameter fit values should scale as $1/s_0^3$. If not, the combined, two-weight fit will have to shift α_s and the DV parameters away from their step-one values. Adding the w_2 FESR at multiple values of s_0 thus provides new constraints on the theory representations.

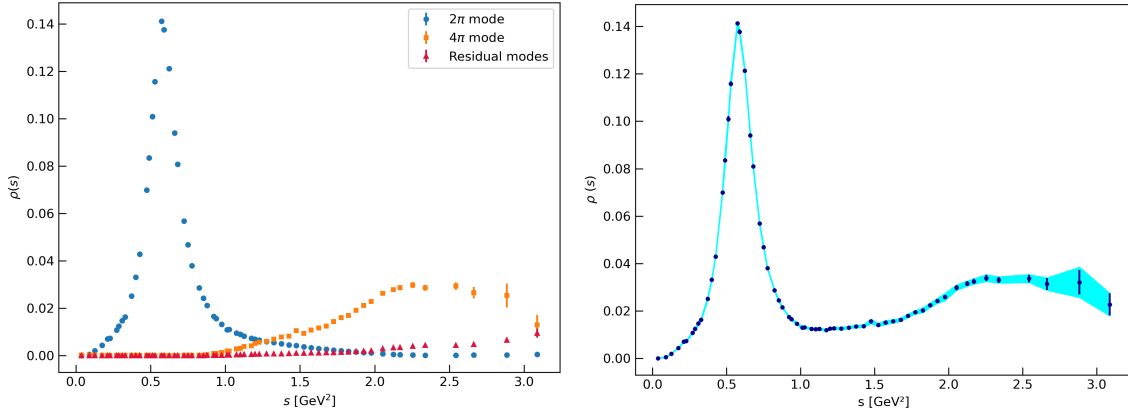


FIG. 8. *The non-strange vector-isovector spectral function, $\rho_{ud;V}(s)$. Left panel: separate 2π , 4π and residual-mode contributions. Right panel: the total inclusive result. The light-blue band represents the inflated errors.*

There is, however, a technical complication to be dealt with in order to access such additional theory-side constraints. Explicitly, for such two-weight fits, it is impossible to perform a standard χ^2 fit when, as in most of the fits we consider, we include all $s_0 > s_0^{\min}$ accessible for our 63-cluster combination. The reason, first pointed out in Ref. [34], and explained in further detail in Ref. [37], is as follows. Consider two sets of spectral integrals, $I_{\text{exp}}^{(w_n)}(s_0)$ and $I_{\text{exp}}^{(w_m)}(s_0)$, sharing a common set of N such s_0 , the first involving weight w_n and the second weight w_m . It turns out that, in this case, only $N + 1$ of these $2N$ integrals are statistically independent. The correlation matrix of the full set is singular, with $N - 1$ eigenvalues exactly equal to zero. This precludes forming the standard χ^2 minimizer. One is left with two options, either to throw out all but one of the second set of spectral integrals and perform a standard χ^2 fit to the resulting reduced $N + 1$ -member set, or retain the full $2N$ -member set, but use a different, non-standard- χ^2 minimizer. The first option has a major disadvantage, namely that, with the reduced spectral integral set containing only one w_m -weighted spectral integral, at a single s_0 , one has no access to the additional theory constraints an analysis including the w_m -weighted spectral integrals at multiple s_0 would have provided. In view of this limitation, we choose option two, retaining the full sets of both spectral integrals and working with a different minimizer.

The alternate minimizer we choose to work with is the block-diagonal quadratic form

$$Q_{nm}^2 = \chi^2(w_n) + \chi^2(w_m), \quad (4.1)$$

with $\chi^2(w_k)$, $k = n, m$, the standard χ^2 function constructed from the data for $I_{\text{exp}}^{(w_k)}(s_0)$ alone, with its $N \times N$ covariance matrix. Correlations between spectral integrals involving different weights are not included in constructing Q^2 , though they are included when obtaining the errors on and correlations among the final fit parameter values.

Focusing on the weights considered in this paper, we note that the theory representation of $I_{\text{exp}}^{(w_0)}(s_0)$ is not sensitive to any of the OPE condensates $C_{D \geq 4}$, while that of $I_{\text{exp}}^{(w_2)}(s_0)$ is sensitive to C_6 , that of $I_{\text{exp}}^{(w_3)}(s_0)$ to C_6 and C_8 , and that of $I_{\text{exp}}^{(w_4)}(s_0)$ to C_6 and C_{10} . Each of the

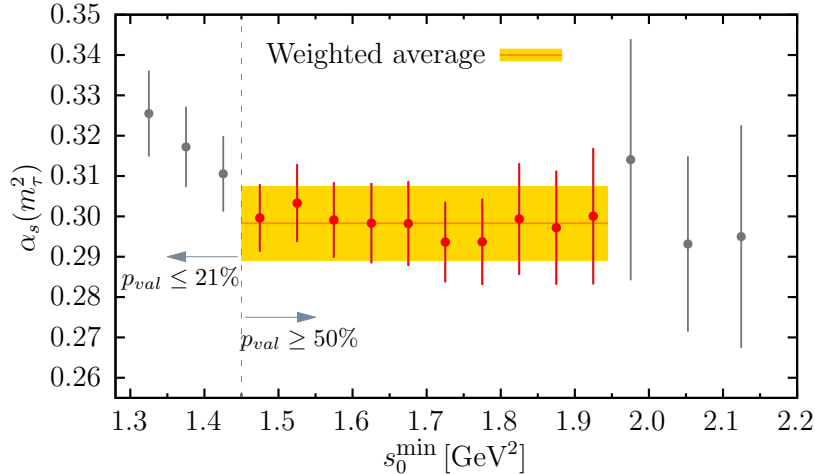


FIG. 9. $\alpha_s(m_\tau^2)$ of Table 2 as a function of s_0^{\min} (showing statistical errors only). The yellow area correspond to the average reported in Eq. (4.2); this average is computed from the data points indicated in red (see text). The thin vertical dashed line separates the regions in which the p -values shown in Table 2 are less than 21% (to the left), from the region where they are greater than 50% (to the right).

corresponding terms in the OPE, Eq. (2.4), has a different s dependence, and thus produces a different s_0 dependence for the associated contour integral. Adding the two-weight fits based on the minimizers Q_{02}^2 , Q_{03}^2 and Q_{04}^2 thus tests for stability of the values of α_s , C_6 and the DV parameters and, indirectly, the reliability of the theoretical representations. Note that the theory-side DV integral contributions have oscillatory s_0 dependences. This is very different from the inverse power dependences, $1/s_0^{D/2}$, of the integrated dimension- D OPE contributions. With oscillatory behavior clearly evident in the experimental spectral function data for $s > 1.5$ GeV² (cf. Fig. 8), both the OPE and DV parts of our theory representation are tested by these two-weight fits.

As noted above, although the “block-diagonal” minimizer defined in Eq. (4.1) does not incorporate the correlations between spectral integrals, $I^{(w_n)}(s_0)$ and $I^{(w_m)}(s_0)$, with different weights, one can still obtain parameter errors for such fits by linear error propagation including the full two-weight covariance matrix [46], and associated p -values using the method of Ref. [80]. In the fits we report in Sec. IV B all parameter errors shown for two-weight fits have been obtained accordingly.

B. Results

In Table 2 we show, as a function of s_0^{\min} , the results of fits to $I_{\text{exp}}^{(w_0)}(s_0)$ for s_0 in a range extending from s_0^{\min} up to the highest s in our 63-cluster set, $s_{\text{max}} = 3.0871$ GeV². We set the parameter c in Eq. (2.9) to zero in this section, but will consider the effect of non-zero values in Sec. IV C below. The dependence of the fit results on s_0^{\min} for $\alpha_s(m_\tau^2)$ and the DV parameters are shown by the black points in Figs. 9 and 10, respectively.

Inspecting the table, we see that fits with s_0^{\min} ranging from 1.4747 to 1.9249 GeV² have good p -values, with parameter values stable over the full range. For smaller s_0^{\min} , the p -

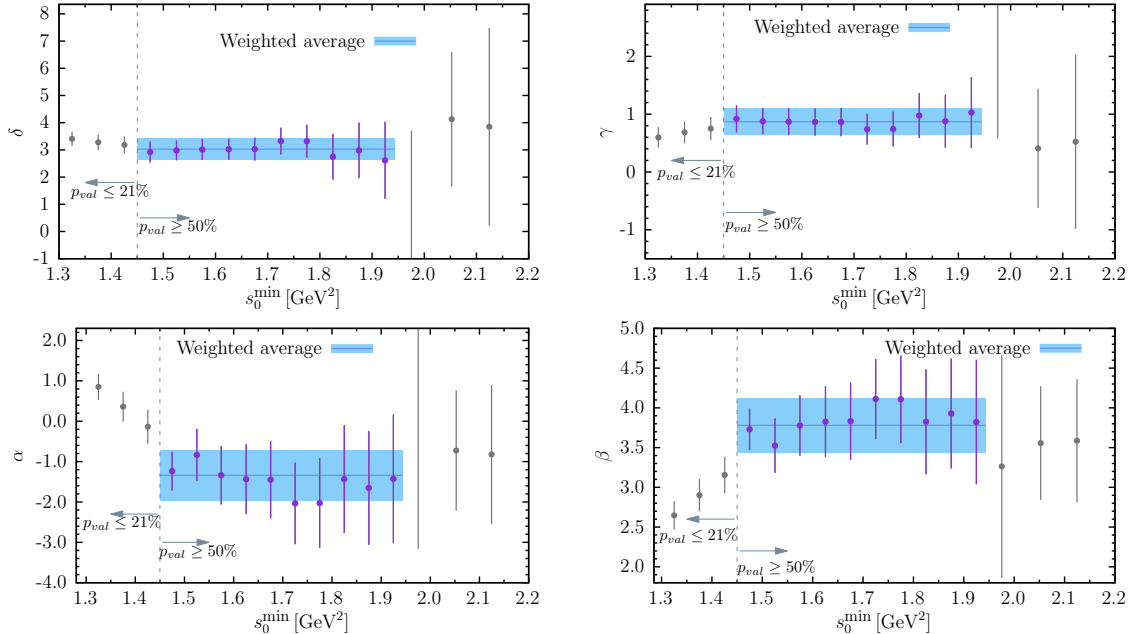


FIG. 10. DV parameters of Table 2 as a function of s_0^{\min} (showing statistical errors only). The blue areas correspond to the averages reported in Eq. (4.2); these averages are computed from the data points indicated in purple (see text). β and γ are in GeV⁻². The thin vertical dashed line separates the regions in which the p -values shown in Table 2 are less than 21% (to the left), from the region where they are greater than 50% (to the right).

values (while acceptable) show a steep drop, and parameter values (notably $\alpha_s(m_\tau^2)$, α and β) are less stable. This suggests that the large- s theoretical representation employed in the fit starts to break down. For s_0^{\min} values greater than 1.9249 GeV², p -values remain good, but parameters are less well determined; parameter errors grow as the number of available data points for each fit decreases.

We have checked how the results for $\alpha_s(m_\tau^2)$ change when we use the spectral function with inflated errors. Over the whole range of s_0^{\min} shown in the table, we find little change in the errors, and no significant impact on the values, obtained for $\alpha_s(m_\tau^2)$. More interesting is what happens if we replace the updated hadronic BFs from Ref. [30] used in the construction of the spectral function with those of the earlier 2019 HFLAV compilation, Ref. [28]. With the older BFs, which had smaller errors, especially for the $\pi^- 3\pi^0$ mode, the errors on $\alpha_s(m_\tau^2)$ for $s_0^{\min} \in [1.4747, 1.9249]$ GeV² become about 6 – 20% smaller. As a consequence, the error on our new value for $\alpha_s(m_\tau^2)$ turns out to be larger than the error on the value obtained in Ref. [9], despite the addition of the high-precision Belle 2π data to the analysis.

We have computed the covariance matrices for the values of α_s and the DV parameters obtained from fits with different s_0^{\min} between 1.4747 and 1.9249 GeV². For our final α_s result, we average the ten values in this range, using a diagonal fit to avoid the possible bias the strong correlations between them might produce. The error on this average, however, is determined by linearly propagating the full α_s covariance matrix. The same averaging

s_0^{\min}	χ^2/dof	$p\text{-val.}$	$\alpha_s(m_\tau^2)$	δ	γ	α	β
1.3250	28.25/18	0.058	0.3255(107)	3.41(27)	0.60(18)	0.85(32)	2.65(18)
1.3752	23.76/17	0.13	0.3172(100)	3.28(30)	0.69(19)	0.36(37)	2.90(20)
1.4254	20.13/16	0.21	0.3106(95)	3.18(32)	0.75(20)	-0.14(42)	3.16(23)
1.4747	10.39/15	0.79	0.2996(84)	2.92(39)	0.92(24)	-1.24(48)	3.73(26)
1.5252	9.36/14	0.81	0.3033(98)	2.98(37)	0.88(23)	-0.84(65)	3.53(34)
1.5747	7.99/13	0.84	0.2991(95)	3.01(39)	0.87(24)	-1.34(73)	3.78(38)
1.6254	7.95/12	0.79	0.2983(102)	3.02(40)	0.87(24)	-1.44(87)	3.83(45)
1.6752	7.95/11	0.72	0.2982(109)	3.03(43)	0.86(25)	-1.45(97)	3.83(49)
1.7251	6.78/10	0.75	0.2936(103)	3.33(50)	0.74(27)	-2.0(1.0)	4.11(52)
1.7750	6.78/9	0.66	0.2937(112)	3.32(61)	0.74(31)	-2.0(1.2)	4.11(57)
1.8250	5.61/8	0.69	0.2994(147)	2.75(85)	0.98(39)	-1.4(1.4)	3.82(68)
1.8750	5.48/7	0.60	0.2972(152)	3.0(1.0)	0.88(46)	-1.7(1.5)	3.93(71)
1.9249	5.31/6	0.50	0.3001(181)	2.6(1.4)	1.03(62)	-1.4(1.7)	3.82(81)
1.9754	4.17/5	0.53	0.3141(186)	0.7(1.5)	1.82(64)	-0.3(1.8)	3.26(89)
2.0526	2.45/4	0.65	0.2932(247)	4.1(1.1)	0.4(1.1)	-0.7(1.6)	3.56(79)
2.1246	2.44/3	0.49	0.2950(252)	3.9(3.0)	0.5(1.3)	-0.8(1.8)	3.59(84)

TABLE 2. Results of fits to $I_{\text{exp}}^{(w_0)}(s_0)$ employing the combined 63-cluster spectral function, with $s_{\text{max}} = 3.0871 \text{ GeV}^2$, s_0^{\min} in GeV^2 and β and γ in GeV^{-2} .

strategy is used for the DV parameters. We find the values (statistical errors only)

$$\begin{aligned}
\alpha_s(m_\tau^2) &= 0.2983(92) , \\
\delta &= 3.03(40) , \\
\gamma &= 0.87(23) \text{ GeV}^{-2} , \\
\alpha &= -1.34(63) , \\
\beta &= 3.78(34) \text{ GeV}^{-2} .
\end{aligned}
\tag{4.2}$$

The final $\alpha_s(m_\tau^2)$ and DV parameter results are shown in yellow in Fig. 9 and blue in Fig. 10, respectively, with statistical errors only. While the errors have been computed using the full covariance matrix for the ten values of each parameter for s_0^{\min} between 1.4747 and 1.9249 GeV^2 in Table 2, we note that taking the errors for the fit with the largest p -value in the table leads to reasonable estimates of the average parameter errors. We will take Eq. (4.2) to define our central results and statistical errors. The systematic error on $\alpha_s(m_\tau^2)$ will be discussed in the following subsection.

For illustrative purposes, the fit to $I_{\text{exp}}^{(w_0)}(s_0)$ for $s_0^{\min} = 1.5747 \text{ GeV}^2$ is displayed in the left panel of Fig. 11. The right panel of the same figure shows a comparison of the representation for $\rho_{ud;V}(s)$ obtained using the parameters of this fit with the combined experimental result obtained in Sec. III.

In Table 3, we present the results for the block-diagonal simultaneous fits to $I_{\text{exp}}^{(w_0)}(s_0)$ and $I_{\text{exp}}^{(w_2)}(s_0)$, limiting ourselves to the ten values of s_0^{\min} used in obtaining the ten-point averages in Eq. (4.2) above. Taking again diagonal averages of the ten values from this interval, we

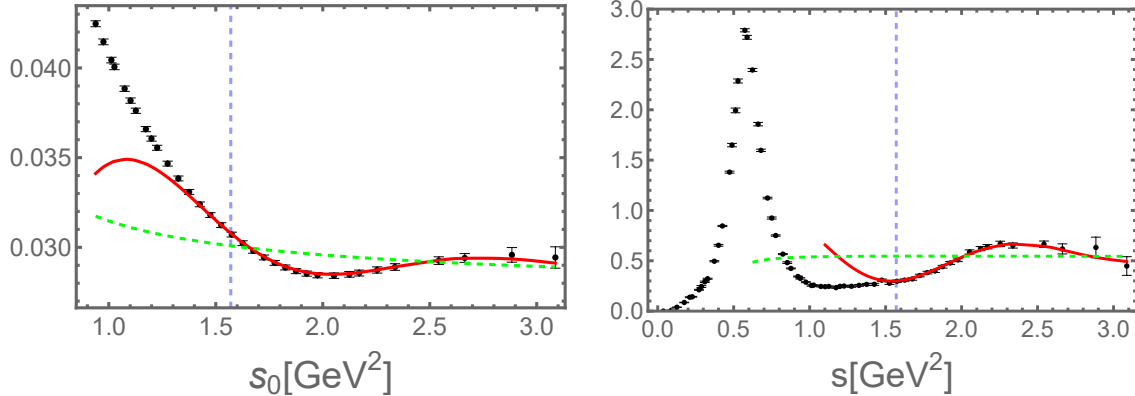


FIG. 11. *Left panel: Comparison of the fitted theoretical representations and the spectral moments $I_{\text{exp}}^{(w_0)}(s_0)$ from the fit with $s_0^{\text{min}} = 1.5747 \text{ GeV}^2$. Right panel: Comparison of $2\pi^2$ times the 63-cluster experimental spectral function and theoretical representation thereof resulting from the fit. The black symbols denote the experimental results, the solid red curves the fitted theory results, and the green dashed curves the OPE parts of the fitted theory curves. The vertical blue dashed lines mark $s = s_0^{\text{min}} = 1.5747 \text{ GeV}^2$.*

find the results

$$\begin{aligned}
 \alpha_s(m_\tau^2) &= 0.2961(91) , \\
 \delta &= 2.73(40) , \\
 \gamma &= 1.05(25) \text{ GeV}^{-2} , \\
 \alpha &= -1.65(65) , \\
 \beta &= 3.95(35) \text{ GeV}^{-2} , \\
 C_6 &= -0.0084(16) \text{ GeV}^6 .
 \end{aligned}
 \tag{4.3}$$

We have chosen the errors for the fit with the largest p -value as the errors for each parameter in Eqs. (4.3). As we will not use the two-weight fits for our central results, this choice is adequate for checking the stability of our fits. The first five parameter values, especially $\alpha_s(m_\tau^2)$, are in good agreement with those in Eq. (4.2), while C_6 appears here for the first time.

As in Ref. [9], in the case of simultaneous block-diagonal fits to $I_{\text{exp}}^{(w_0)}(s_0)$ and either $I_{\text{exp}}^{(w_3)}(s_0)$ or $I_{\text{exp}}^{(w_4)}(s_0)$, we find that the correlation matrices for the spectral moments with the doubly pinched weights w_n , with $n = 3$ or 4 , have very small eigenvalues, around 10^{-10} , three orders of magnitude smaller than the smallest eigenvalue for the set of $I_{\text{exp}}^{(w_2)}(s_0)$ or $I_{\text{exp}}^{(w_0)}(s_0)$ integrals. We find that if we “thin” the set of integrals used in the fit, starting at a given s_0^{min} and including only every second, third, *etc.*, of the available higher s_0 , the Q^2/dof values drop rapidly to a value below 1, and the fit stabilizes as we increase the degree of thinning. Tables 4 and 5 show the results of these fits for the cases $n = 3$ and $n = 4$, thinning the data in these cases by a factor three.

In the tables for the two-weight fits involving the doubly pinched weights, we see that the results fluctuate a little more than in the corresponding parts of Tables 2 and 3. The reason is that, because of the thinning, the sets of s_0 values used for the three fits starting at, for

s_0^{\min}	Q_{02}^2/dof	$p\text{-val.}$	$\alpha_s(m_\tau^2)$	δ	γ	α	β	$10^2 C_6$
1.4747	33.96/34	0.31	0.2976(83)	2.64(40)	1.09(24)	-1.43(48)	3.83(27)	-0.79(13)
1.5252	30.97/32	0.33	0.2992(91)	2.72(40)	1.04(25)	-1.32(65)	3.78(35)	-0.77(16)
1.5747	29.11/30	0.32	0.2960(90)	2.73(41)	1.04(25)	-1.76(73)	4.00(39)	-0.85(15)
1.6254	28.96/28	0.25	0.2954(95)	2.76(42)	1.03(25)	-1.86(89)	4.05(46)	-0.86(17)
1.6752	28.23/26	0.21	0.2947(98)	2.83(44)	1.00(26)	-1.99(97)	4.11(50)	-0.89(17)
1.7251	27.03/24	0.18	0.2919(97)	3.01(52)	0.92(28)	-2.39(1.06)	4.30(54)	-0.95(17)
1.7750	26.60/22	0.13	0.2932(109)	2.84(66)	1.00(33)	-2.21(1.24)	4.21(62)	-0.92(21)
1.8250	24.41/20	0.12	0.2979(140)	2.30(89)	1.22(41)	-1.64(1.53)	3.94(76)	-0.79(33)
1.8750	24.40/18	0.08	0.2978(153)	2.3(1.2)	1.22(55)	-1.7(1.7)	3.95(85)	-0.80(38)
1.9249	22.61/16	0.07	0.3034(195)	1.3(1.6)	1.66(68)	-1.2(2.2)	3.7(1.1)	-0.60(57)

TABLE 3. Results of combined fits to $I_{\text{exp}}^{(w_0)}(s_0)$ and $I_{\text{exp}}^{(w_2)}(s_0)$ employing our 63-cluster spectral function, with $s_{\text{max}} = 3.0869 \text{ GeV}^2$, s_0^{\min} in GeV^2 , β and γ in GeV^{-2} and C_6 in GeV^6 .

s_0^{\min}	Q_{03}^2/dof	$p\text{-val.}$	$\alpha_s(m_\tau^2)$	δ	γ	α	β	$10^2 C_6$	$10^2 C_8$
1.4747	3.22/7	0.35	0.3053(96)	3.22(40)	0.72(25)	-1.11(60)	3.66(32)	-0.71(16)	1.15(27)
1.5252	8.14/7	0.07	0.2999(90)	3.06(41)	0.83(25)	-1.75(71)	4.00(38)	-0.84(14)	1.40(25)
1.5747	1.95/5	0.24	0.2997(92)	3.27(39)	0.71(23)	-1.79(75)	4.01(39)	-0.84(14)	1.40(25)
1.6254	1.65/5	0.27	0.3001(103)	3.40(44)	0.65(26)	-1.71(88)	3.96(45)	-0.83(17)	1.41(31)
1.6752	3.63/5	0.10	0.2901(88)	3.41(48)	0.69(27)	-3.18(95)	4.70(48)	-1.04(12)	1.81(22)
1.7251	0.75/3	0.001	0.2927(95)	3.75(64)	0.50(33)	-2.7(1.0)	4.45(50)	-0.99(15)	1.71(28)
1.7750	1.04/3	0.003	0.3085(181)	2.9(1.1)	0.85(49)	-0.9(1.5)	3.54(75)	-0.63(44)	0.99(91)
1.8250	1.01/3	0.02	0.3104(257)	1.5(1.7)	1.53(74)	-0.7(2.5)	3.5(1.2)	-0.52(76)	0.6(1.8)

TABLE 4. Results of combined fits to $I_{\text{exp}}^{(w_0)}(s_0)$ and $I_{\text{exp}}^{(w_3)}(s_0)$ employing our 63-cluster spectral function, with $s_{\text{max}} = 3.0869 \text{ GeV}^2$, s_0^{\min} in GeV^2 , β and γ in GeV^{-2} , C_6 in GeV^6 and C_8 in GeV^8 . In the fits, the data for $I_{\text{exp}}^{(w_0)}(s_0)$ and $I_{\text{exp}}^{(w_3)}(s_0)$ have been thinned by a factor 3.

example, $s_0^{\min} = 1.5747, 1.6254$ and 1.6752 GeV^2 are different. The integrals $I_{\text{exp}}^{(w_{3,4})}(s_0 = 1.6254)$ and $I_{\text{exp}}^{(w_{3,4})}(s_0 = 1.6752)$ are not part of the fit starting with $I_{\text{exp}}^{(w_{3,4})}(s_0 = 1.5747)$ whereas, if the data were not thinned, they would be.¹⁸

Because of the thinning, the fits for $s_0^{\min} = 1.7251, 1.7750$ and 1.8250 GeV^2 are based on very few degrees of freedom, and thus tend to be less stable; p -values for these fits drop steeply from those for fits with smaller s_0^{\min} values. Fits with $s_0^{\min} = 1.8750 \text{ GeV}^2$ and higher have only one degree of freedom, and are very unstable. We thus take the parameter

¹⁸ Of course, this does *not* mean that the data used in these three fits are fully independent, because all $I_{\text{exp}}^{(w)}(s_0)$ are strongly correlated, especially for nearby s_0 values.

s_0^{\min}	Q_{04}^2/dof	$p\text{-val.}$	$\alpha_s(m_\tau^2)$	δ	γ	α	β	$10^2 C_6$	$10^2 C_{10}$
1.4747	2.96/7	0.39	0.3052(96)	3.22(40)	0.72(25)	-1.10(60)	3.66(32)	-0.69(16)	1.33(42)
1.5252	8.02/7	0.07	0.2998(91)	3.07(40)	0.82(25)	-1.72(71)	3.99(38)	-0.82(15)	1.75(42)
1.5747	1.72/5	0.27	0.2996(93)	3.27(39)	0.71(23)	-1.77(76)	4.00(40)	-0.82(15)	1.79(43)
1.6254	1.50/5	0.29	0.3000(103)	3.40(44)	0.65(26)	-1.69(88)	3.95(45)	-0.82(18)	1.81(53)
1.6752	3.58/5	0.11	0.2900(88)	3.41(48)	0.69(27)	-3.16(95)	4.69(48)	-1.03(13)	2.54(40)
1.7251	0.61/3	0.002	0.2926(96)	3.72(65)	0.51(33)	-2.7(1.0)	4.44(50)	-0.98(15)	2.38(52)
1.7750	0.85/3	0.008	0.3091(189)	2.9(1.1)	0.88(49)	-0.8(1.6)	3.50(77)	-0.59(48)	0.9(1.9)
1.8250	0.91/3	0.03	0.3112(266)	1.4(1.8)	1.56(75)	-0.6(2.5)	3.4(1.3)	-0.47(82)	-0.2(4.4)

TABLE 5. Results of combined fits to $I_{\text{exp}}^{(w_0)}(s_0)$ and $I_{\text{exp}}^{(w_4)}(s_0)$ employing the 63-cluster spectral function, with $s_{\text{max}} = 3.0869 \text{ GeV}^2$, s_0^{\min} in GeV^2 , β and γ in GeV^{-2} , C_6 in GeV^6 and C_{10} in GeV^{10} . In the fits, the data for $I_{\text{exp}}^{(w_0)}(s_0)$ and $I_{\text{exp}}^{(w_4)}(s_0)$ have been thinned by a factor 3.

averages only over the fits for the first five s_0^{\min} values shown in the tables, and obtain

	w_0	$w_0 \ \& \ w_2$	$w_0 \ \& \ w_3$	$w_0 \ \& \ w_4$	
$\alpha_s(m_\tau^2)$	0.2983(92)	0.2961(91)	0.2987(96)	0.2986(96)	
δ	3.03(40)	2.73(40)	3.26(40)	3.26(40)	
γ	0.87(23)	1.05(25)	0.72(25)	0.72(25)	
α	-1.34(63)	-1.65(65)	-1.73(60)	-1.71(60)	(4.4)
β	3.78(34)	3.95(35)	3.99(32)	3.98(32)	
C_6		-0.0084(16)	-0.0087(16)	-0.0085(16)	
C_8			0.0147(27)		
C_{10}				0.0186(42)	

In this equation, we have, for ease of comparison also listed the values obtained in Eqs. (4.2) and (4.3). We recall that the errors in the w_0 column have been obtained from the full covariance matrix for each parameter, while those in the other three columns are rough estimates obtained by taking the errors for the fit with the largest p -value in each of the tables.

Comparing the parameter values in Eq. (4.4), we see that the values obtained are consistent across all these fits, in particular for the OPE parameters $\alpha_s(m_\tau^2)$ and C_6 . The DV parameter values for the two-weight fits agree with the central values of the w_0 fit, within the errors on that fit.

C. Analysis and comparison with Ref. [9]

We begin with a comparison between our new result

$$\alpha_s(m_\tau^2) = 0.2983(92)_{\text{stat}} , \quad (4.5)$$

given in Eq. (4.2) and that obtained in Ref. [9], which is (showing the statistical error only)

$$\alpha_s(m_\tau^2) = 0.3077(65)_{\text{stat}} . \quad (4.6)$$

The new central value is lower, and the new error larger. In order to probe possible reasons for these differences, we carried out several other fits. First, we considered what happens if the Belle 2π data are omitted from the combination, and the BFs of Ref. [28] are used instead of the updated ones of Ref. [30]. This allows for a direct comparison with the result from Ref. [9], which also employed only ALEPH and OPAL data and HFLAV 2019 BF input, but used a different data combination algorithm. This yields

$$\alpha_s(m_\tau^2) = 0.3075(84)_{\text{stat}} \quad 2019 \text{ BFs; without Belle data .} \quad (4.7)$$

The central value is very close to that of Eq. (4.6), but the error is larger.¹⁹ This implies that the new data-combination algorithm leads to somewhat larger statistical errors than that of Eq. (4.6). Of course, with only the $\pi^-\pi^0$ mode available from Belle, we are forced to use the new algorithm if the goal is to include the Belle data. We also note that our treatment of the 4π modes is less reliant on the poorly determined off-diagonal covariances of the ALEPH and OPAL 4π data than was that of Ref. [9], with the OPAL $\pi^-3\pi^0$ data now included through a diagonal fit. This also leads to some increase in the statistical error on $\alpha_s(m_\tau^2)$.

Next, we considered what happens if we add the Belle 2π data, keeping BFs from Ref. [28] instead of Ref. [30]. This yields

$$\alpha_s(m_\tau^2) = 0.3055(81)_{\text{stat}} \quad 2019 \text{ BFs; with Belle data .} \quad (4.8)$$

Finally, we also give the result obtained without Belle data, but using the 2022 BFs of Ref. [30]:

$$\alpha_s(m_\tau^2) = 0.3001(97)_{\text{stat}} \quad 2022 \text{ BFs; without Belle data .} \quad (4.9)$$

Comparing Eqs. (4.2), (4.7), (4.8) and (4.9) we see that the use of the new BFs has two effects: central values with the new HFLAV BFs are clearly smaller, and errors are larger. The latter is no surprise since the updated BF $B_{\pi^-3\pi^0}$ has an error a factor of 2.4 larger. We also see that including the Belle data somewhat lowers the central value for $\alpha_s(m_\tau^2)$, but this effect is much smaller than the impact of the switch from 2019 to 2022 HFLAV BFs. We conclude that the change from the 2020 result in Eq. (4.6) to the new result in Eq. (4.5) is caused by changes in the input data, and not by a change in our methodology, witness the good agreement between Eq. (4.6) and Eq. (4.7). A visual summary of the above explorations is provided in Fig. 12, which displays the results obtained for α_s using the various experimental and BF inputs, and data combination methodologies, run up to the $n_f = 5$ scale $\mu = m_Z$.

Next, we turn to a discussion of systematics. The error on $\alpha_s(m_\tau^2)$ in our central determination, Eq. (4.2) is statistical only. This leaves several systematic effects to be accounted for. First, we take the spread of values in Eq. (4.4), 0.0026, as our measure of the fit-dependence systematic error. We also, as in Ref. [9], vary the perturbative coefficient c_{51} by $\pm 50\%$ (*cf.* Sec. II). This leads to a (symmetrized) variation of $\alpha_s(m_\tau^2)$ of ± 0.0022 (at $s_0^{\text{min}} = 1.5747 \text{ GeV}^2$), which we treat as an additional theory error.²⁰ We also considered the variation obtained from choosing the scale μ^2 in Eq. (2.5) equal to either $2s_0$ or m_τ^2 , instead of s_0 . The larger of the two resulting scale-change variations, 0.0021, which comes from the

¹⁹ Also the DV parameters from this fit are in excellent agreement with those of Ref. [9].

²⁰ As in Ref. [9], alternate error estimates based on removing order- α_s^5 terms (*i.e.*, setting $c_{5m} = 0$), or removing both order- α_s^4 and order- α_s^5 terms (*i.e.*, setting both $c_{4m} = 0$ and $c_{5m} = 0$) lead to differences equal to or smaller than the differences obtained from the 50% variation in c_{51} .

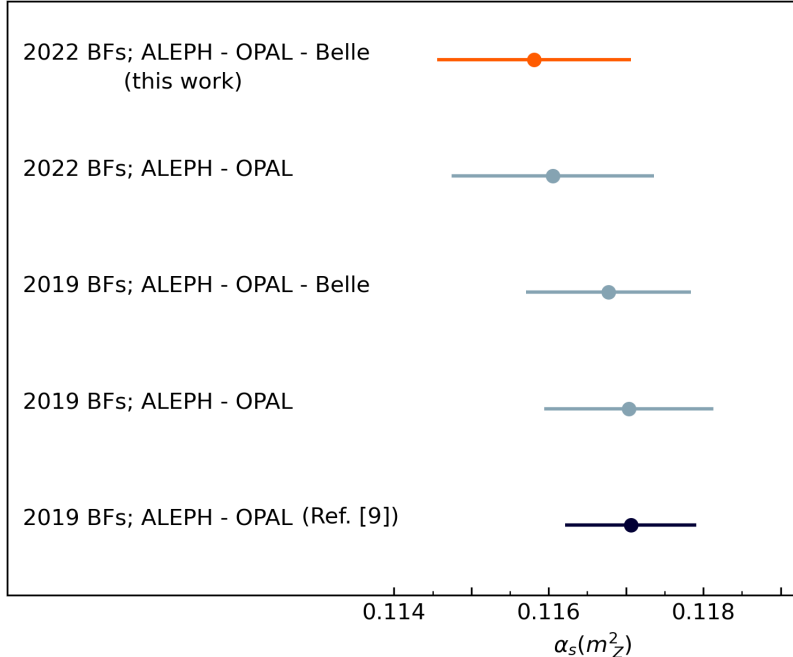


FIG. 12. Results for $\alpha_s(m_Z^2)$ using different choices for the 2π data sets included, the input 2π and 4π BFs, and the data combination methodology employed. All results except the black point are from this work; the black point is the final result from Ref. [9]. Errors shown are statistical only.

choice $\mu^2 = 2s_0$, is (slightly) smaller than the estimate obtained from varying c_{51} . We thus take the larger, ± 0.0022 , value as our estimate for the systematic error resulting from the truncation of perturbation theory.

As discussed in Ref. [9], since the different weights have different levels of pinching, and thus different levels of DV suppression, as well as different weightings of neglected α_s -suppressed logarithmic corrections to higher-dimension OPE contributions, the variation of the central values for $\alpha_s(m_\tau^2)$ shown in Eq. (4.4) can be taken as an indication of the uncertainties resulting from possible shortcomings in the modeling of NP effects. This variation, 0.0026, is only 0.9% of the value of $\alpha_s(m_\tau^2)$ in Eq. (4.2) and much smaller than the total statistical error of 3.1%.

Possible corrections to the DV parametrization in Eq. (2.9), as well as logarithmic corrections to the OPE coefficients, were analyzed in Ref. [37] and found to be safely negligible for the α_s determination based on the spectral function of Ref. [9]. That study, following Ref. [65], investigated the correction of order $1/s$ in the DV *ansatz* (2.9), finding that, while the single-weight, w_0 FESR yielded χ^2/dof and α_s essentially constant over a wide range of $c > 0$, the χ^2/dof of the fit and stability of the α_s determination both deteriorated rapidly for c more negative than about -1 GeV^2 . A rapid deterioration was also found in the consistency of the w_0 and w_2 FESRs as c became more negative than -1 GeV^2 [37].²¹ The results of fits to the spectral integrals, $I_{\text{exp}}^{(w_0)}(s_0)$, constructed from the new spectral function, with $s_0^{\text{min}} = 1.5747 \text{ GeV}^2$ and variable c , are shown in Fig. 13. The left panel shows the χ^2 values

²¹ For further details on these points, see Appendix C of Ref. [37].

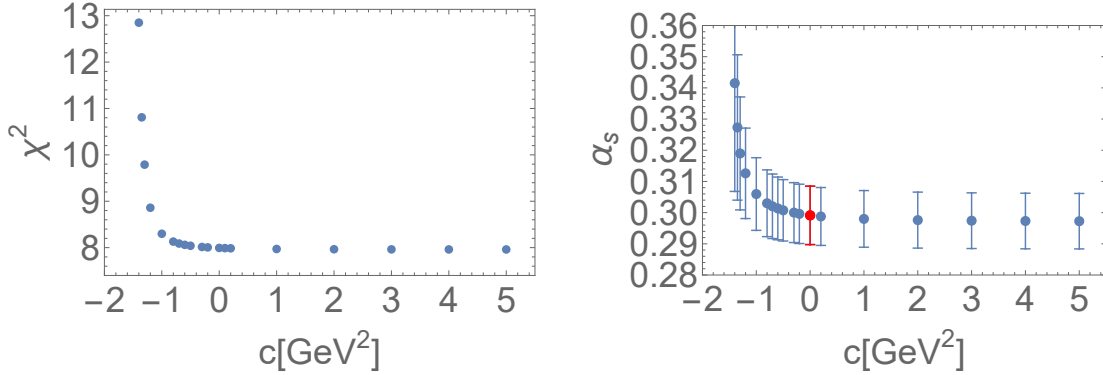


FIG. 13. The results of fits at $s_0^{\min} = 1.5747 \text{ GeV}^2$ using the ansatz (2.9) for DVs, as a function of the parameter c (in GeV^2). The left and right panels show the dependences of χ^2 and $\alpha_s(m_\tau^2)$ on c , respectively. The red point in the right panel corresponds to the value of $\alpha_s(m_\tau^2)$ in Table 2.

and the right panel the $\alpha_s(m_\tau^2)$ values, both as a function of c .²² Taking c negative is seen to lead to a rapid deterioration of the fit quality, while $\alpha_s(m_\tau^2)$ is essentially independent of c for positive c , even for values well outside the range for which the term c/s in Eq. (2.9) is a small correction. The conclusions regarding such a possible sub-leading correction to our DV ansatz are thus the same as those found previously in Ref. [37] using the spectral function of Ref. [9]. Although the results of fits using combinations of weights with different degrees of pinching, and hence different weightings of DV contributions, show, at the current level of precision, no evidence for a significant systematic uncertainty resulting from choosing $c = 0$, we, nonetheless, assign a systematic error to this choice, obtained by varying c over the range $\pm 0.8 \text{ GeV}^2$, which corresponds to a c/s correction in Eq. (2.9) of about 50% at the lowest value of s_0^{\min} used in the determination of $\alpha_s(m_\tau^2)$. This leads to an additional systematic error of -0.0010 for $c > 0$ and $+0.0039$ for $c < 0$.

Combining all errors leads to our final result:

$$\begin{aligned} \alpha_s(m_\tau^2) &= 0.2983 \pm 0.0092_{\text{stat}} \pm 0.0026_{\text{fit}} \pm 0.0022_{\text{pert}} \pm 0.0025_c \\ &= 0.2983 \pm 0.0101 \quad (n_f = 3) , \end{aligned} \quad (4.10)$$

where we symmetrized the error due to the c/s correction in Eq. (2.9).²³ This can be compared with our final result from Ref. [9],

$$\begin{aligned} \alpha_s(m_\tau^2) &= 0.3077 \pm 0.0065_{\text{stat}} \pm 0.0038_{\text{pert}} \\ &= 0.3077 \pm 0.0075 . \end{aligned} \quad (4.11)$$

Note that the earlier, 2020 value does not include an estimate of the uncertainty associated with possible sub-leading corrections to the leading DV ansatz since no study involving variation of the sub-leading contribution parameter, c , was considered in Ref. [9].²⁴ The errors in Eqs. (4.10) and (4.11) are, of course, not uncorrelated, so the two results should

²² For analogous results produced using the spectral function of Ref. [9], see Fig. 2 of Ref. [37].

²³ Without the c/s -correction error, the total error would be ± 0.0098 .

²⁴ Including the ± 0.0025 version of the estimate for this uncertainty obtained above using the new spectral function would increase the error on this earlier determination from ± 0.0075 to about ± 0.0080 .

not be interpreted as agreeing within errors. The reason for the difference, as explained above, is the change in input data, notably the update of the 2π and 4π BF's by HFLAV.

Running the result of Eq. (4.10) to the Z -mass scale using the standard self-consistent combination of five-loop running [61, 62] with four-loop matching [81, 82] at the charm and bottom thresholds ($2m_c(m_c)$ and $2m_b(m_b)$), respectively, with $\overline{\text{MS}}$ masses from the PDG [1]), we obtain the corresponding $n_f = 5$ result

$$\alpha_s(m_Z^2) = 0.1159 \pm 0.0014 \quad (n_f = 5) . \quad (4.12)$$

With five-loop running and four-loop matching the uncertainty due to the running is very small.²⁵

V. CONCLUSION

Our goal in this paper was to include more of the world's data for hadronic τ decays into the τ -based determination of the strong coupling α_s from the inclusive, non-strange vector-isovector hadronic spectral function. Previously, we combined ALEPH [4] and OPAL [5] data for the decays $\tau \rightarrow \pi^- \pi^0 \nu_\tau$, $\tau \rightarrow 2\pi^- \pi^+ \pi^0 \nu_\tau$ and $\tau \rightarrow \pi^- 3\pi^0 \nu_\tau$, supplemented with mostly electroproduction data and CVC²⁶ to obtain the residual-mode contributions [9]. As we first combined the 2π and 4π data for each of these two experiments before combining the resulting single-experiment sums, this did not allow for the inclusion of $\pi^- \pi^0$ data from Belle [6] and CLEO [7, 8], since no 4π -mode results are available from those experiments. In this paper we therefore changed our algorithm for combining data from different experiments to first perform single-mode, all-experiment combinations of the 2π data and 4π data separately, thus allowing us to include Belle and CLEO data in the 2π combination as well as in the construction of the inclusive, non-strange vector-isovector hadronic spectral function, $\rho_{ud;V}(s)$. We found that inclusion of the Belle data has a significant impact on the combined spectral function. In contrast, as discussed in App. B, the impact of including the CLEO data is small and, since no complete information is available on the CLEO systematic errors, we did not include the CLEO data in the construction of our final result for $\rho_{ud;V}(s)$.

In addition to including hadronic τ -decay data from more experiments, we have also updated the values for the input $\pi^- \pi^0$, $2\pi^- \pi^+ \pi^0$ and $\pi^- 3\pi^0$ branching fractions with those of Ref. [30]. This has a significant effect on the precision of $\rho_{ud;V}(s)$ and the strong coupling since the new HFLAV value for the $\pi^- 3\pi^0$ branching fraction is significantly lower, and has a much larger error than, the earlier values reported in Ref. [28]. In contrast, there have been no relevant improvements to the electroproduction data used for the residual-mode input in Ref. [9], and we thus carried over the residual-mode distributions unchanged from Ref. [9].

The main results of our paper are a new determination of the inclusive, non-strange vector-isovector hadronic spectral function from the world's available data for hadronic τ decays, and a new determination of $\alpha_s(m_\tau^2)$ from this spectral function through finite-energy sum rules. The new spectral function is tabulated in Table 1, and shown in Fig. 8. Our new result for the $n_f = 3$ coupling, $\alpha_s(m_\tau^2)$, can be found in Eq. (4.10), and the conversion of this result to the corresponding $n_f = 5$ value at the Z mass in Eq. (4.12). Our results

²⁵ An an example, performing the matching at $m_c(m_c)$ and $m_b(m_b)$ rather than $2m_c(m_c)$ and $2m_b(m_b)$ produces a shift of just 0.00008, which does not contribute to the final uncertainty.

²⁶ Together with $K\bar{K}$ τ -decay mode distribution data measured by BaBar [10].

are consistent with those of Ref. [9], though it should be kept in mind that the current and Ref. [9] results are correlated, as they are based on overlapping data sets. The new central value of $\alpha_s(m_\tau^2)$ is 0.0094 lower than that of Ref. [9]. As can be seen by comparing Eq. (4.5) with Eqs. (4.8) and (4.9), almost 80% of this downward shift is due to the HFLAV update of the 2π and 4π BF's, with roughly 20% due to the inclusion of the Belle 2π data. We note, in particular, that applying our new data combination method to the data used in Ref. [9] leads to a result fully compatible with that of Ref. [9], as a comparison of Eqs. (4.6) and (4.7) shows.

We also note that the statistical error (and thus, since the systematic error is basically unchanged, the combined error) on our new result for $\alpha_s(m_\tau^2)$ is larger than in Ref. [9]. The main reason for this increase is again the inclusion of new experimental information: the Belle 2π data, and the updated branching fractions. While the Belle data in principle add significantly more information about the 2π mode, inclusion of these data necessitated a change in the combination algorithm which turned out to produce an increase in the error on α_s . The changes in the new algorithm also include a treatment of the 4π data which is less reliant on poorly determined ALEPH and OPAL 4π correlations. As can be seen by comparing Eq. (4.6) and Eq. (4.7), the change in algorithm leads to a statistical error larger by about 30%. The error on $\alpha_s(m_\tau^2)$ has also increased as a result of the larger errors on the updated HFLAV 2022 BF's, especially that of the $\pi^-3\pi^0$ mode. Clearly, a high-statistics Belle II determination of the two 4π unit-normalized distributions would have the potential to significantly improve the error situation, as would improved determinations of the 4π BF's, especially that of the $\pi^-3\pi^0$ mode. In fact, already a high-statistics determination of the experimentally less challenging $2\pi^-\pi^+\pi^0$ distribution would be of interest in this regard, as this mode constitutes about 80% (by BF) of the sum of the two 4π -mode contributions.

A further reason improved τ -decay determinations of the $2\pi^-\pi^+\pi^0$ - and $\pi^-3\pi^0$ -mode contributions to $\rho_{ud;V}(s)$ would be of interest is the connection to the $2\pi^+2\pi^-$ and $\pi^+\pi^-2\pi^0$ contributions to the electromagnetic (EM) neutral vector, isovector-current spectral function, $\rho_{EM}^{I=1}(s)$, which are determined by the corresponding electroproduction cross sections and play an important role in the dispersive determination of the hadronic vacuum polarization contribution to the anomalous magnetic moment of the muon. In the isospin limit, the Pais relations [83] provide expressions for the exclusive-mode 4π contributions to $\rho_{ud;V}(s)$ in terms of the exclusive-mode 4π contributions to $\rho_{EM}^{I=1}(s)$, with the $\pi^-3\pi^0$ τ contribution determined by the $2\pi^+2\pi^-$ EM contribution, and the $2\pi^-\pi^+\pi^0$ τ contribution by a complementary linear combination of the EM $2\pi^+2\pi^-$ and $\pi^+\pi^-2\pi^0$ contributions. The Pais-relation expectations obtained using publicly available exclusive-mode EM 4π results from the compilation of Ref. [84], have errors ranging from a factor of ~ 2 smaller than those of corresponding ALEPH and OPAL τ combination for s near 2 GeV^2 to $\sim 5 - 6$ smaller near the τ kinematic endpoint. There are, however, signs of non-trivial tensions at a scale larger than those of the $\sim 1\%$ or so deviations expected due to isospin-breaking corrections to the Pais relations, between the central values and s -dependences of the τ data and the Pais-relation expectations in this same region, albeit with point-by-point significances limited by the significantly larger τ errors. Post-LEP-era improvements to the τ 4π distributions would be of significant interest in this context.

Our new value for α_s represents the current best value obtained from the world's data for hadronic τ decays, and supersedes the value of Ref. [9]. The result is farther from the world average [1] than that found in Ref. [9]. The reason for the shift is the inclusion of new data, with the shift to a lower value being dominated by the change in the 4π branching

fractions.

The determination of α_s from τ decays is kinematically limited by the τ mass, and because of its relatively low value, non-perturbative effects in QCD have to be accounted for. Some, but not all, of the non-perturbative effects are captured by the OPE, as the OPE does not account for the oscillatory resonance behavior clearly seen in the spectral function at values of s in the region between 2 GeV^2 and m_τ^2 (*cf.* Fig. 8). Any determination of α_s from τ decays thus needs to consider the possibility that residual DV contributions may not be entirely numerically negligible in the FESRs used in that determination. We have investigated this issue using the *ansatz*, Eq. (2.9), to describe violations of quark-hadron duality. The form of this *ansatz* is based on the presumed Regge-like behavior of the resonance spectrum at large s , combined with insights from large- N_c QCD [65].²⁷ The multi-weight, multi- s_0 fits detailed in Sec. IV B provide non-trivial tests of this DV model since (i) the differently weighted theory integrals have different sensitivities to duality violations and (ii) integrated DV and non-perturbative OPE contributions have very different s_0 dependences.²⁸ A new test is the sensitivity to a subleading correction represented by the c/s term in Eq. (2.9), shown in Fig. 13. Our systematic error estimate now takes into account the effect of such a possible subleading correction, increasing the total error on our result for $\alpha_s(m_\tau^2)$ by about 3%.

The issue of duality violations, however, still needs to be studied in more detail. We first comment that, as more data for hadronic τ decays become available in the future, our current analysis framework makes it straightforward to take these new data into account. Increased precision can help in testing the theoretical representations used on the theory side of the FESRs in the analysis more stringently. An alternate approach would be to employ recently developed techniques for obtaining weighted integrals of the spectral function from lattice QCD, using, for example, the method of Ref. [85]. A major advantage of the alternate approach is the absence of the kinematic restriction to $s_0 \leq m_\tau^2$ which is unavoidable for analyses based on experimental data of the type employed in this paper. We plan to investigate this approach in the near future.

Acknowledgments

We thank Hisaki Hayashii for discussion of the Belle data, Sven Menke for discussion of the OPAL data, and Jon Urheim for discussion of the CLEO data. We also thank Mattia Bruno for discussion of Ref. [80]. LMM would like to thank the Department of Physics and Astronomy at San Francisco State University for hospitality. DB's work was supported by the São Paulo Research Foundation (FAPESP) grant No. 2021/06756-6 and by CNPq grant No. 308979/2021-4. AE and MG are supported by the U.S. Department of Energy, Office of Science, Office of High Energy Physics, under Award No. DE-SC0013682. KM is supported by a grant from the Natural Sciences and Engineering Research Council of Canada. LMM is supported by FAPESP grants No. 2023/08482-6 and No. 2022/16553-8. SP is supported by the Spanish Ministerio de Ciencia e Innovacion, grants PID2020-112965GB-I00 and PID2023-146142NB-I00, and by the Departament de Recerca i Universitats from Generalitat de Catalunya to the Grup de Recerca 00649 (Codi: 2021 SGR 00649). IFAE is partially funded by the CERCA program of the Generalitat de Catalunya.

²⁷ Further discussion of our assumptions can be found in Ref. [37].

²⁸ For more tests also including OPAL or ALEPH axial-vector data, we refer to Refs. [47, 48].

Appendix A: Approximate d’Agostini bias correction

In this Appendix, we review briefly how global normalization constants, with their associated uncertainties, can lead to a d’Agostini bias in the fitted results [45] for the 4π -mode data combination. In addition, we present the adaptation of the NNPDF procedure of Ref. [79] employed in our 4π -mode combination to approximately avoid this bias.

As explained in Sec. III D, it turns out to be possible to combine only the separate, already summed, ALEPH and OPAL $2\pi^-\pi^+\pi^0$ plus $\pi^-3\pi^0$ mode contribution totals. This implies that we need to multiply the kinematic-weight-rescaled exclusive-mode unit-normalized distributions from ALEPH and OPAL by the corresponding BFs (divided by \mathcal{F}) before carrying out the fit combining all 4π data. As these BFs have non-zero errors, the combination suffers from a potential d’Agostini bias.

If we wish to combine the spectral data for a certain exclusive mode for two experiments k and ℓ , we start by constructing the exclusive-mode spectral functions $\rho_i^{k,\ell}$ from the kinematic-weight-rescaled unit-normalized distributions $u_i^{k,\ell}$. This involves multiplying by the BF B and the factor $1/\mathcal{F}$ with \mathcal{F} given in Eq. (3.4) (the index i labels the bins for each experiment):

$$\rho_i^k = \frac{B}{\mathcal{F}} u_i^k . \quad (\text{A1})$$

With c_{ij}^k the covariance matrix for the distributions u_i^k , the covariance matrix for ρ^k is given by

$$\text{cov}_{ij}^{kk} = \frac{B^2}{\mathcal{F}^2} c_{ij}^k + \frac{1}{\mathcal{F}^2} u_i^k u_j^k \sigma_B^2 + \frac{B^2}{\mathcal{F}^4} u_i^k u_j^k \sigma_{\mathcal{F}}^2 , \quad (\text{A2})$$

where σ_B is the error on B and $\sigma_{\mathcal{F}}$ the error on \mathcal{F} .²⁹ The errors on B and \mathcal{F} also induce covariances between data for the same mode from two different experiments k and ℓ of the form

$$\text{cov}_{ij}^{k\ell} = \frac{1}{\mathcal{F}^2} u_i^k u_j^\ell \sigma_B^2 + \frac{B^2}{\mathcal{F}^4} u_i^k u_j^\ell \sigma_{\mathcal{F}}^2 . \quad (\text{A3})$$

The presence of terms in Eq. (A2) and Eq. (A3) that depend on $u_i^k u_j^k$ and $u_i^k u_j^\ell$ leads to a potential d’Agostini bias when we combine the spectral functions ρ_i^k for the two 4π modes: data points with higher values of the distribution u_i^k have less impact on the determination of the $\rho^{(m)}(s)$ cluster results in the fitted combination. In other words, this bias leads to our combined spectral function, $\rho^{(m)}(s)$ having lower central values than one would have obtained if σ_B and $\sigma_{\mathcal{F}}$ were to be negligibly small [45, 79].

In Ref. [79], an iterative procedure was proposed to minimize the effect of the d’Agostini bias. The idea is to iterate the fit by, at each step of the iteration, replacing the original data u_i^m in Eqs. (A2) and (A3) by the corresponding result from the previous iteration of the fit, *i.e.*, by $\rho^{(m)}(s)/(B/\mathcal{F})$, interpolated to the bins of the experiments k and ℓ , redoing the fit with this as updated input. As explained in detail in Ref. [79], this iterative procedure is expected to converge rapidly.

For the 2π mode, the bias problem can be avoided by directly combining unit-normalized spectral data from different experiments (in our case, ALEPH, OPAL and Belle). However, the ill-behaved covariance matrices for the $2\pi^-\pi^+\pi^0$ and $\pi^-3\pi^0$ modes force us to first form the full two-mode 4π sums, $\rho_{4\pi}(s) = \rho_{2\pi^-\pi^+\pi^0}(s) + \rho_{\pi^-3\pi^0}(s)$, for each of ALEPH and OPAL, and only then combine the data from the two experiments. It follows that after the first step

²⁹ We neglect correlations between u_i^k , B and \mathcal{F} .

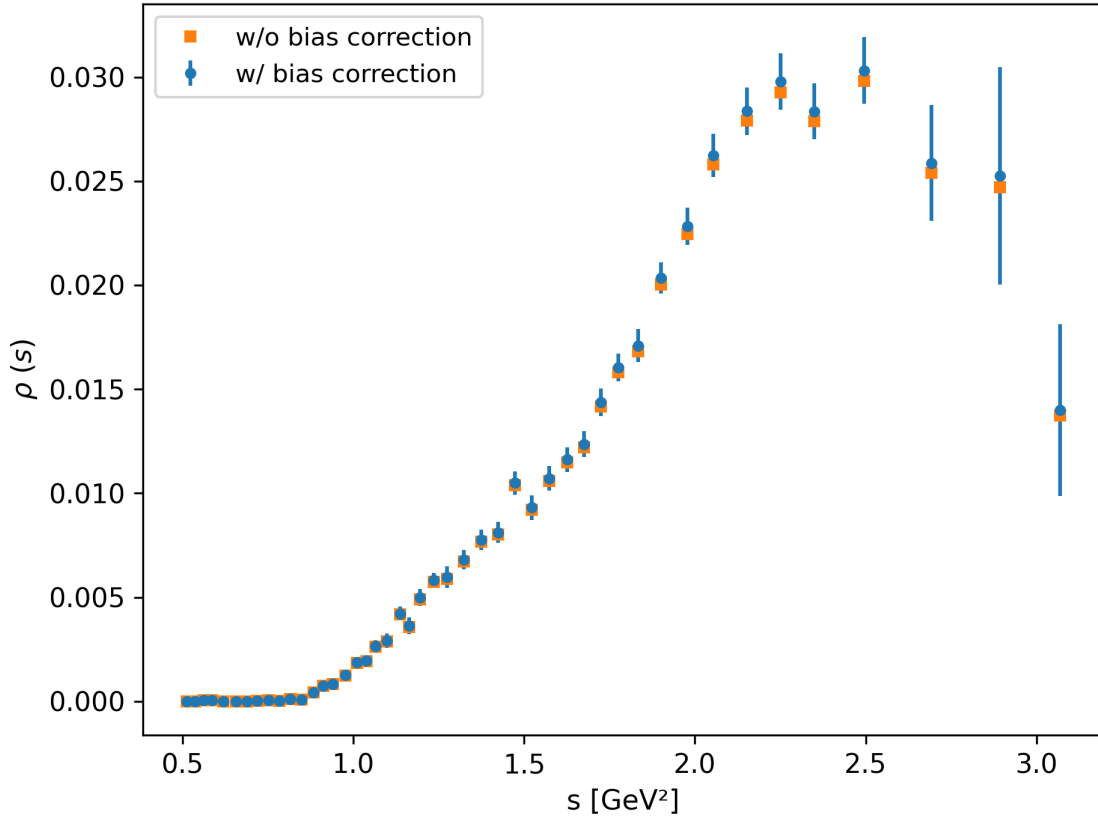


FIG. 14. The 4π combined spectral function, with (blue points) and without (orange points) bias correction.

in the iteration we have only the combined “clustered” spectral function $[\rho_{4\pi}]^{(m)}(s)$, and no longer have information about the precise contribution from the individual $2\pi^-\pi^+\pi^0$ and $\pi^-3\pi^0$ modes. In order to iterate the fit we use the following approximate procedure. We first interpolate $[\rho_{4\pi}]^{(m)}(s)$ to the ALEPH and OPAL bins, thus constructing “improved” ALEPH and OPAL 4π spectral distributions. Then, in order to turn this into “improved” ALEPH and OPAL $2\pi^-\pi^+\pi^0$ and $\pi^-3\pi^0$ distributions, we split these 4π distributions according to the bin-by-bin ratios for these two modes for each of the two experiments. This then allows us to carry out the iterative procedure proposed by Ref. [79]. We find convergence after two steps. This procedure is approximate, because it rests on the assumption that keeping the ratios of the original ALEPH and OPAL experimental data between the two modes the same during the iteration procedure is a reasonable approximation. We note that these ratios are not exactly the same for ALEPH and OPAL.

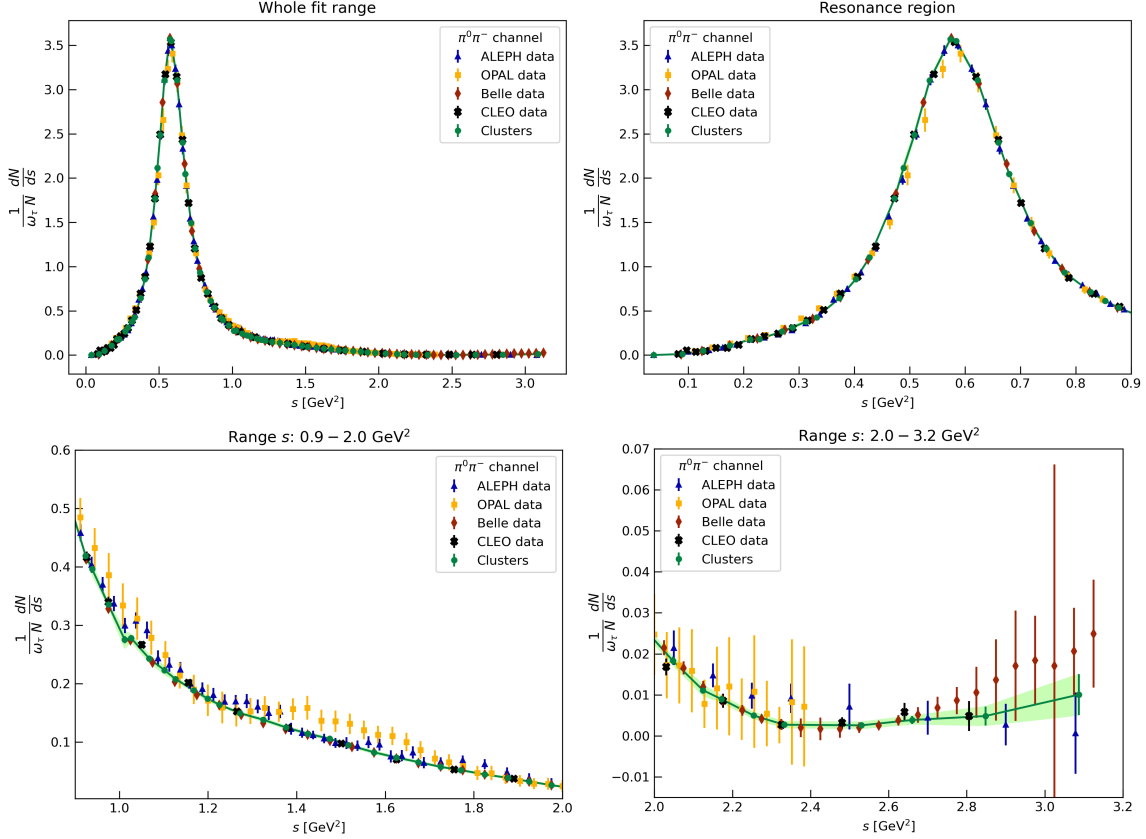


FIG. 15. The 2π unit-normalized number distribution combination, divided by $w_T(s)$, together with the data from the individual ALEPH, OPAL, Belle and CLEO experiments. The error bars represent the uninflated errors, while inflated errors are represented by the green band.

Appendix B: Inclusion of the CLEO $\pi^-\pi^0$ -mode data

In this appendix, we investigate the effect of including the CLEO data for the $\tau \rightarrow \pi^-\pi^0\nu_\tau$ decay mode [7, 8] in the construction of the combined 2π spectral function.

For this data set, only statistical errors, but not systematic errors, are available on a bin-by-bin basis. This raises the question as to whether the CLEO data can be reliably combined with the other three data sets, for which both statistical and systematic covariance information is available. In this appendix, we nevertheless include the CLEO data set in a four-experiment combination of the $\pi^-\pi^0$ mode, using only the statistical error information available for CLEO, to see to what extent the CLEO data modify the combination. Starting from the unit-normalized number distributions from all four experiments, we follow the same strategy as used in Sec. III C. The resulting unit-normalized number distribution, divided by the kinematic weight $w_T(s)$, is shown in Fig. 15. We use the same number of clusters, 63, and assign the CLEO data points to the clusters with the nearest invariant-mass-squared value. Since they are determined from Eq. (3.8), the cluster s values for the new combination are not identical to those for the combination of Sec. III C, but they are close, as can be seen

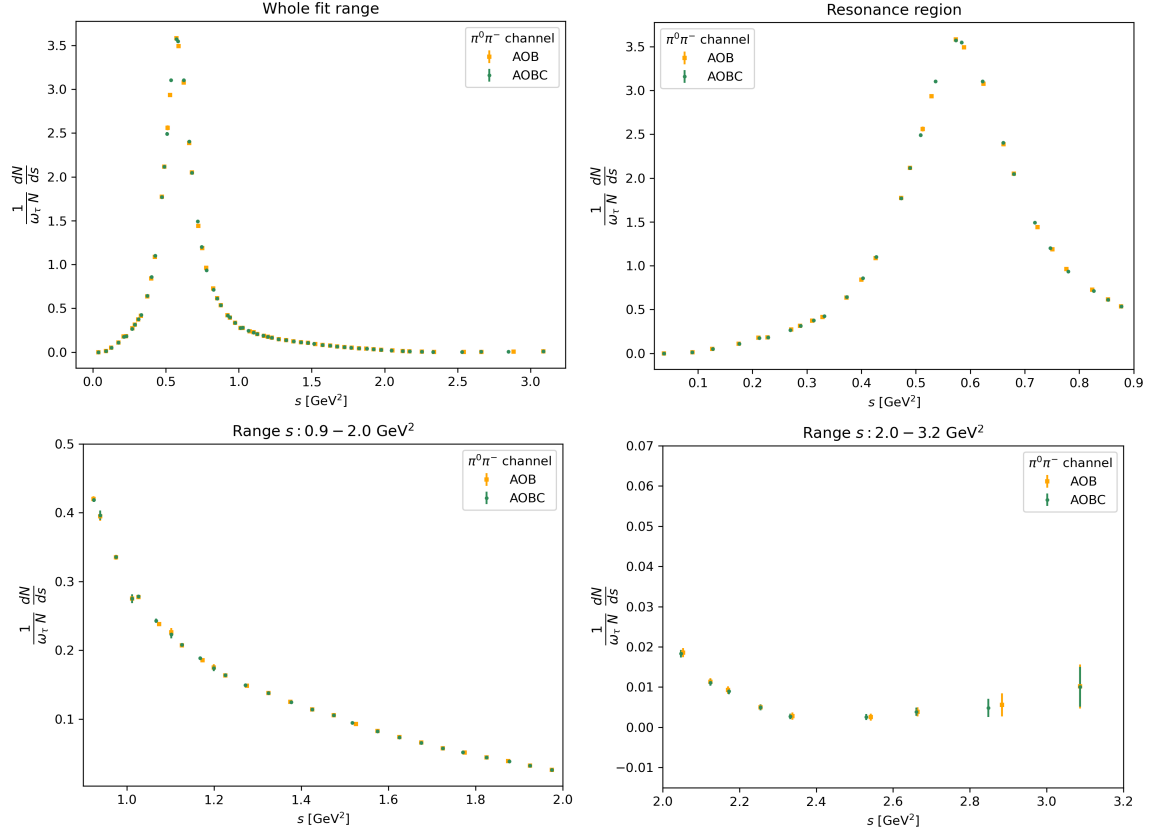


FIG. 16. Comparison of the 2π unit-normalized number distribution combination (divided by $w_T(s)$) with orange points indicating the ALEPH, OPAL and Belle combination (AOB) of Sec. III, and green points indicating the ALEPH, OPAL, Belle and CLEO combination (AOBC).

in Fig. 16. This figure shows the $\pi^-\pi^0$ unit-normalized number distribution combination, divided by $w_T(s)$, with (AOBC, green points) and without (AOB, orange points) the CLEO data. From the figure, it can be seen that the CLEO data have a rather limited effect on the combined 2π spectrum. The global fit is of good quality, with $\chi^2 = 201$ for 193 degrees of freedom, and a p -value of 0.34. The local p -values per cluster are very similar to those shown in Fig. 2.

We have also investigated the effect of including the CLEO data in our inclusive combined non-strange V spectral function on the values for $\alpha_s(m_\tau^2)$ and the DV parameters. It turns out that the effect is very small. As an example, consider the fit to $I_{\text{ex}}^{(w_0)}(s_0)$ with $s_0^{\text{min}} = 1.5747 \text{ GeV}^2$, which has a p -value of 0.84 and leads to the parameter values

$$\begin{aligned}
 \alpha_s(m_\tau^2) &= 0.2997(96) , \\
 \delta &= 3.04(39) , \\
 \gamma &= 0.85(24) \text{ GeV}^{-2} , \\
 \alpha &= -1.30(73) , \\
 \beta &= 3.76(38) \text{ GeV}^{-2} .
 \end{aligned}
 \tag{B1}$$

Both central values and errors are very close to the corresponding entries in Table 2. In particular, we see that inclusion of the CLEO data does not increase the precision that can be obtained from the fit to the combined spectral function. This remains true for the parameter values obtained with the other s_0^{\min} values in the range used to produce our result (4.2).

Given these results, and given the fact that no complete covariance information is available for the CLEO $\pi^-\pi^0$ data set, we do not include the CLEO data in producing our central results, Table 1 for the inclusive vector isovector spectral function, and Eq. (4.10) for the value of $\alpha_s(m_\tau^2)$.

Appendix C: Combination of 2π and 4π spectral distributions

We begin by grouping the data together into a single vector [86],

$$d_0 = (u_{2\pi,i}, u_{1\pi^0,i}, u_{3\pi^0,i}, B_{2\pi}, B_{1\pi^0}, B_{3\pi^0}, \mathcal{F}) , \quad (\text{C1})$$

where u_X indicates a kinematic-weight-rescaled unit-normalized spectral distribution, and $X = 2\pi, 1\pi^0$ and $3\pi^0$ are short forms for the $\pi^-\pi^0$, $2\pi^-\pi^+\pi^0$ and $\pi^-3\pi^0$ exclusive modes, respectively. The B_X are the corresponding BFs given in Eq. (3.5), \mathcal{F} is the combination of external constants given in Eq. (3.4), and $u_{2\pi}$ is the full combined 2π kinematic-weight-rescaled version of the unit-normalized 2π distribution obtained in Sec. III C. The quantities $u_{1\pi^0,i}$ and $u_{3\pi^0,i}$, in contrast, are the unions, for each of the two 4π exclusive modes, of the ALEPH and OPAL kinematic-weight-rescaled unit-normalized spectral distribution data, *before* performing the two-mode combination described in Sec. III D. If the total numbers of ALEPH and OPAL $1\pi^0$ and $3\pi^0$ data points are N_1 and N_3 , respectively, the length of d_0 is $63 + N_1 + N_3 + 3 + 1$. The covariance matrix C_0 for Eq. (C1) is block diagonal, containing the blocks for the 2π combined 63×63 covariance matrix $C_{2\pi}$, the merged ALEPH and OPAL $N_1 \times N_1$ $1\pi^0$ and $N_3 \times N_3$ $3\pi^0$ covariance matrices as in Sec. III D, the 3×3 covariance matrix for the BFs constructed from Eq. (3.5), and the squared-error for \mathcal{F} in the last diagonal entry.³⁰

These data can be combined into the spectral data vector

$$d_1 = \frac{1}{\mathcal{F}} (B_{2\pi}u_{2\pi,i}, B_{1\pi^0}u_{1\pi^0,i}, B_{3\pi^0}u_{3\pi^0,i}) . \quad (\text{C2})$$

With D_1 the rectangular matrix of derivatives of the entries of Eq. (C2) with respect to those of Eq. (C1),

$$D_1 = \frac{1}{\mathcal{F}} \begin{pmatrix} B_{2\pi}\delta_{ij} & 0 & 0 & u_{2\pi,i} & 0 & 0 & -B_{2\pi}u_{2\pi,i}/\mathcal{F} \\ 0 & B_{1\pi^0}\delta_{ij} & 0 & 0 & u_{1\pi^0,i} & 0 & -B_{1\pi^0}u_{1\pi^0,i}/\mathcal{F} \\ 0 & 0 & B_{3\pi^0}\delta_{ij} & 0 & 0 & u_{3\pi^0,i} & -B_{3\pi^0}u_{3\pi^0,i}/\mathcal{F} \end{pmatrix} , \quad (\text{C3})$$

the $(63 + N_1 + N_3) \times (63 + N_1 + N_3)$ covariance matrix C_1 for d_1 is given by

$$C_1 = D_1 C_0 D_1^T . \quad (\text{C4})$$

We note that C_1 is no longer block-diagonal, because of the form of D_1 .

³⁰ Because the relative error on B_e is very small ($O(0.1\%)$) we can neglect the correlations between B_e and the hadronic BFs.

In the next step, we apply a transformation to d_1 to arrive at

$$d_2 = \begin{pmatrix} \rho_{2\pi} \\ \rho_{4\pi} \end{pmatrix}, \quad (\text{C5})$$

where $\rho_{2\pi} = B_{2\pi} u_{2\pi} / \mathcal{F}$ is the 2π spectral function obtained in Sec. III C, *i.e.*, the first entry of d_1 , and

$$\rho_{4\pi} = M_{4\pi} \frac{1}{\mathcal{F}} \begin{pmatrix} B_{1\pi^0} u_{1\pi^0, i} \\ B_{3\pi^0} u_{3\pi^0, i} \end{pmatrix}, \quad (\text{C6})$$

with $M_{4\pi}$ the $46 \times (N_1 + N_3)$ rectangular matrix, defined in Eq. (3.17), which combines the ALEPH and OPAL 4π data into the 46-cluster combined two-mode 4π spectral function sum. We thus have that

$$d_2 = D_2 d_1^T \quad (\text{C7})$$

(the transpose appears because we gave d_1 as a row vector), with

$$D_2 = \begin{pmatrix} \mathbf{1} & 0 \\ 0 & M_{4\pi} \end{pmatrix}, \quad (\text{C8})$$

in which $\mathbf{1}$ is the 63×63 unit matrix. The covariance matrix for d_2 is

$$C_2 = D_2 C_1 D_2^T. \quad (\text{C9})$$

Finally, we linearly interpolate the 4π spectral function $\rho_{4\pi}$ to the s values of the 63 2π clusters, and add the interpolated $\rho_{4\pi}$ to $\rho_{2\pi}$. The covariances of the resulting $2\pi + 4\pi$ spectral function, $\rho_{2\pi+4\pi}$, are straightforwardly obtainable from C_2 and the coefficients used to interpolate the 4π results from the s values of the 46-cluster 4π s set to those of the 63-cluster 2π set. We emphasize that the matrix C_0 contains all data covariances, and that, when parts of it are modified in the fit of Sec. III D; all correlations are retained in the error propagation.

-
- [1] S. Navas *et al.* [Particle Data Group], *Review of particle physics*, Phys. Rev. D **110**, no.3, 030001 (2024).
 - [2] R. Barate *et al.* [ALEPH Collaboration], *Measurement of the spectral functions of axial-vector hadronic tau decays and determination of $\alpha(S)(M^{*2}(\tau))$* , Eur. Phys. J. C **4**, 409 (1998).
 - [3] S. Schael *et al.* [ALEPH Collaboration], *Branching ratios and spectral functions of tau decays: Final ALEPH measurements and physics implications*, Phys. Rept. **421**, 191 (2005) [arXiv:hep-ex/0506072].
 - [4] M. Davier, A. Hoecker, B. Malaescu, C. Z. Yuan and Z. Zhang, *Update of the ALEPH non-strange spectral functions from hadronic τ decays*, Eur. Phys. J. C **74**, 2803 (2014) [arXiv:1312.1501 [hep-ex]].
 - [5] K. Ackerstaff *et al.* [OPAL Collaboration], *Measurement of the strong coupling constant $\alpha(s)$ and the vector and axial-vector spectral functions in hadronic tau decays*, Eur. Phys. J. C **7**, 571 (1999) [arXiv:hep-ex/9808019].
 - [6] M. Fujikawa *et al.* [Belle], *High-Statistics Study of the $\tau^- \rightarrow \pi^- \pi^0 \nu(\tau)$ Decay*, Phys. Rev. D **78**, 072006 (2008) [arXiv:0805.3773 [hep-ex]].

- [7] T. Coan *et al.* [CLEO], *Measurement of α_s from tau decays*, Phys. Lett. B **356**, 580 (1995).
- [8] S. Anderson *et al.* [CLEO], *Hadronic structure in the decay $\tau \rightarrow \pi^- \pi^0 \nu(\text{tau})$* , Phys. Rev. D **61**, 112002 (2000) [arXiv:hep-ex/9910046 [hep-ex]].
- [9] D. Boito, M. Golterman, K. Maltman, S. Peris, M. V. Rodrigues and W. Schaaf, *Strong coupling from an improved τ vector isovector spectral function*, Phys. Rev. D **103**, no.3, 034028 (2021) [arXiv:2012.10440 [hep-ph]].
- [10] J. P. Lees *et al.* [BaBar Collaboration], *Measurement of the spectra function for the $\tau^- \rightarrow K^- K_S \nu_\tau$ decay*, Phys. Rev. D **98**, 032010 (2018) [arXiv:1806.10280 [hep-ex]].
- [11] M. Achasov *et al.* [SND Collaboration], *Updated measurement of the $e^+e^- \rightarrow \omega \pi^0 \rightarrow \pi^0 \pi^0 \gamma$ cross section with the SND detector*, Phys. Rev. D **94**, 112001 (2016) [arXiv:1610.00235 [hep-ex]].
- [12] J. P. Lees *et al.* [BaBar Collaboration], *Measurement of the $e^+e^- \rightarrow \pi^+ \pi^- \pi^0 \pi^0$ cross section using initial-state radiation at BABAR*, Phys. Rev. D **96**, 092009 (2017) [arXiv:1709.01171 [hep-ex]].
- [13] K. Inami, *et al.* [Belle Collaboration], *Precise measurement of hadronic tau-decays with an eta meson*, Phys. Lett. B **672**, 209 (2009) [arXiv:0811.0088 [hep-ex]].
- [14] V. M. Aulchenko, *et al.* [SND Collaboration], *Measurement of the $e^+e^- \rightarrow \eta \pi^+ \pi^-$ cross section in the center-of-mass energy range 1.22-2.00 GeV with the SND detector at the VEPP-2000 collider*, Phys. Rev. D **91**, 052013 (2015) [arXiv:1412.1971 [hep-ex]].
- [15] M. N. Achasov, *et al.* [SND Collaboration], *Measurement of the $e^+e^- \rightarrow \eta \pi^+ \pi^-$ cross section with the SND detector at the VEPP-2000 collider*, Phys. Rev. D **97**, 012008 (2018) [arXiv:1711.08862 [hep-ex]].
- [16] J. P. Lees, *et al.* [BaBar Collaboration], *Study of the process $e^+e^- \rightarrow \pi^+ \pi^- \eta$ using initial state radiation*, Phys. Rev. D **97**, 052007 (2018) [arXiv:1801.02960 [hep-ex]].
- [17] S. S. Griбанov, *et al.*, *Measurement of the $e^+e^- \rightarrow \eta \pi^+ \pi^-$ cross section with the CMD-3 detector at the VEPP-2000 collider*, JHEP **01**, 112 (2020) [arXiv:1907.08002 [hep-ex]].
- [18] We thank Sergei Griбанov for providing the inverse error matrix for the $\eta \pi \pi$ results of Ref. [17].
- [19] B. Aubert, *et al.* [BaBar Collaboration], *Measurements of $e^+e^- \rightarrow K^+ K^- \eta$, $K^+ K^- \pi^0$ and $K_S^0 K^\pm \pi^\mp$ cross sections using initial state radiation events*, Phys. Rev. D **77**, 092002 (2008) [arXiv:0710.4451 [hep-ex]].
- [20] B. Aubert, *et al.* [BaBar Collaboration], *The $e^+e^- \rightarrow 3(\pi^+ \pi^-)$, $2(\pi^+ \pi^- \pi^0)$ and $K^+ K^- 2(\pi^+ \pi^-)$ cross sections at center-of-mass energies from production threshold to 4.5 GeV measured with initial-state radiation*, Phys. Rev. D **73**, 052003 (2006) [arXiv:hep-ex/0602006].
- [21] We thank Eugeny Solodov for providing tables of these cross sections, which are shown in Figures 18 and 19 of Ref. [20], but not explicitly tabulated there.
- [22] P. A. Lukin, *et al.* [CMD-3 Collaboration], *Study of the process $e^+e^- \rightarrow 3(\pi^+ \pi^-)$ in the C.M. energy range 1.5-2.0 GeV with the CMD-3 detector*, Phys. Lett. B **723**, 82 (2013) [arXiv:1302.0053 [hep-ex]].
- [23] R. R. Akhmetshin, *et al.* [CMD-3 Collaboration], *Study of the process $e^+e^- \rightarrow \pi^+ \pi^- \pi^0 \eta$ in the c.m. energy range 1394-2005 MeV with the CMD-3 detector*, Phys. Lett. B **773**, 150 (2017) [arXiv:1706.06267 [hep-ex]].
- [24] M. N. Achasov, *et al.* [SND Collaboration], *Recent results from SND detector at VEPP-2000 collider*, EPJ Web Conf. **212**, 04002 (2019)
- [25] M. N. Achasov, *et al.* [SND Collaboration], *Measurement of the $e^+e^- \rightarrow \pi^+ \pi^- \pi^0 \eta$ cross section below $\sqrt{s} = 2$ GeV*, Phys. Rev. D **99**, 112004 (2019) [arXiv:1903.09307 [hep-ex]].
- [26] J. P. Lees, *et al.* [BaBar Collaboration], *Study of the reactions $e^+e^- \rightarrow \pi^+ \pi^- \pi^0 \pi^0 \pi^0 \gamma$ and*

- $\pi^+\pi^-\pi^0\pi^0\eta\gamma$ at center-of-mass energies from threshold to 4.35 GeV using initial-state radiation, Phys. Rev. D **98**, 112015 (2018) [arXiv:1810.11962 [hep-ex]].
- [27] B. Aubert, *et al.* [BaBar Collaboration], *The $e^+e^- \rightarrow 2(\pi^+\pi^-)\pi^0$, $2(\pi^+\pi^-)\eta$, $K^+K^-\pi^+\pi^-\pi^0$ and $K^+K^-\pi^+\pi^-\eta$ cross sections measured with initial-state radiation*, Phys. Rev. D **76**, 092005 (2007) (Erratum *ibid.* **77**, 119902 (2008)) [arXiv:0708.2461 [hep-ex]].
- [28] Y. Amhis, *et al.* [HFLLAV Collaboration], *Averages of b-hadron, c-hadron and τ -lepton properties as of 2018*, arXiv:1909.12524 [hep-ex].
- [29] A. Keshavarzi, D. Nomura and T. Teubner, *Muon $g-2$ and $\alpha(M_Z^2)$: a new data-based analysis*, Phys. Rev. D **97**, no.11, 114025 (2018) [arXiv:1802.02995 [hep-ph]].
- [30] Y. S. Amhis *et al.* [HFLLAV], *Averages of b-hadron, c-hadron, and τ -lepton properties as of 2021*, Phys. Rev. D **107**, no.5, 052008 (2023) [arXiv:2206.07501 [hep-ex]].
- [31] M. Davier, S. Descotes-Genon, A. Höcker, B. Malaescu and Z. Zhang, *The determination of α_s from tau decays revisited*, Eur. Phys. J. C **56**, 305 (2008) [arXiv:0803.0979 [hep-ph]].
- [32] P. A. Baikov, K. G. Chetyrkin and J. H. Kühn, *Order α_s^4 QCD Corrections to Z and τ Decays*, Phys. Rev. Lett. **101**, 012002 (2008) [arXiv:0801.1821 [hep-ph]].
- [33] A. Pich and A. Rodríguez-Sánchez, *Determination of the QCD coupling from ALEPH τ decay data*, Phys. Rev. D **94**, 034027 (2016) [arXiv:1605.06830 [hep-ph]].
- [34] A. Pich and A. Rodríguez-Sánchez, *Violations of quark-hadron duality in low-energy determinations of α_s* , JHEP **07**, 145 (2022) [arXiv:2205.07587 [hep-ph]].
- [35] D. Boito, M. Golterman, K. Maltman and S. Peris, *Strong coupling from hadronic τ decays: A critical appraisal*, Phys. Rev. D **95**, 034024 (2017) [arXiv:1611.03457 [hep-ph]].
- [36] D. Boito, M. Golterman, K. Maltman and S. Peris, *Evidence against naive truncations of the OPE from $e^+e^- \rightarrow$ hadrons below charm*, Phys. Rev. D **100**, 074009 (2019) [arXiv:1907.03360 [hep-ph]].
- [37] D. Boito, M. Golterman, K. Maltman and S. Peris, *Quark-hadron duality and the determination of α_s from hadronic τ decay: facts vs. myths*, [arXiv:2402.05588 [hep-ph]].
- [38] A. A. Pivovarov, *Renormalization group analysis of the tau-lepton decay within QCD*, Z. Phys. C **53**, 461 (1992) [Sov. J. Nucl. Phys. **54**, 676 (1991)] [Yad. Fiz. **54**, 1114 (1991)] [arXiv:hep-ph/0302003].
- [39] F. Le Diberder and A. Pich, *The perturbative QCD prediction to $R(\tau)$ revisited*, Phys. Lett. B **286**, 147 (1992).
- [40] A. H. Hoang and C. Regner, *Borel representation of τ hadronic spectral function moments in contour-improved perturbation theory*, Phys. Rev. D **105**, no.9, 096023 (2022) [arXiv:2008.00578 [hep-ph]].
- [41] M. Golterman, K. Maltman and S. Peris, *Difference between fixed-order and contour-improved perturbation theory*, Phys. Rev. D **108**, no.1, 014007 (2023) [arXiv:2305.10386 [hep-ph]].
- [42] N. G. Gracia, A. H. Hoang and V. Mateu, *Mathematical aspects of the asymptotic expansion in contour improved perturbation theory for hadronic tau decays*, Phys. Rev. D **108**, no.3, 034013 (2023) [arXiv:2305.10288 [hep-ph]].
- [43] M. A. Benitez-Rathgeb, D. Boito, A. H. Hoang and M. Jamin, *Reconciling the contour-improved and fixed-order approaches for τ hadronic spectral moments. Part I. Renormalon-free gluon condensate scheme*, JHEP **07**, 016 (2022) [arXiv:2202.10957 [hep-ph]].
- [44] M. A. Benitez-Rathgeb, D. Boito, A. H. Hoang and M. Jamin, *Reconciling the contour-improved and fixed-order approaches for τ hadronic spectral moments. Part II. Renormalon norm and application in α_s determinations*, JHEP **09**, 223 (2022) [arXiv:2207.01116 [hep-ph]].
- [45] G. D'Agostini, *On the use of the covariance matrix to fit correlated data*, Nucl. Instrum. Meth.

- A **346**, 306 (1994).
- [46] D. Boito, O. Catà, M. Golterman, M. Jamin, K. Maltman, J. Osborne and S. Peris, *A new determination of α_s from hadronic τ decays*, Phys. Rev. D **84**, 113006 (2011) [arXiv:1110.1127 [hep-ph]].
 - [47] D. Boito, M. Golterman, M. Jamin, A. Mahdavi, K. Maltman, J. Osborne and S. Peris, *An Updated determination of α_s from τ decays*, Phys. Rev. D **85**, 093015 (2012) [arXiv:1203.3146 [hep-ph]].
 - [48] D. Boito, M. Golterman, K. Maltman, J. Osborne and S. Peris, *The strong coupling from the revised ALEPH data for hadronic τ decays*, Phys. Rev. D **91**, 034003 (2015) [arXiv:1410.3528 [hep-ph]].
 - [49] R. Shankar, *Determination of the Quark-Gluon Coupling Constant*, Phys. Rev. D **15**, 755 (1977).
 - [50] R. G. Moorhouse, M. R. Pennington and G. G. Ross, *What Can Asymptotic Freedom Say About $e^+e^- \rightarrow$ Hadrons?*, Nucl. Phys. B **124**, 285 (1977).
 - [51] K. G. Chetyrkin and N. V. Krasnikov, *Constraints on the Behavior of the e^+e^- Hadron Annihilation Cross-Section in Asymptotically Free Theories and in Theories with Anomalous Dimensions*, Nucl. Phys. B **119**, 174 (1977).
 - [52] K. G. Chetyrkin, N. V. Krasnikov and A. N. Tavkhelidze, *Finite Energy Sum Rules for the Cross-Section of e^+e^- Annihilation Into Hadrons in QCD*, Phys. Lett. B **76**, 83 (1978).
 - [53] N. V. Krasnikov, A. A. Pivovarov and N. N. Tavkhelidze, *The Use of Finite Energy Sum Rules for the Description of the Hadronic Properties of QCD*, Z. Phys. C **19**, 301 (1983).
 - [54] E. G. Floratos, S. Narison and E. de Rafael, *Spectral Function Sum Rules in Quantum Chromodynamics. 1. Charged Currents Sector*, Nucl. Phys. B **155**, 115 (1979).
 - [55] R. A. Bertlmann, G. Launer and E. de Rafael, *Gaussian Sum Rules in Quantum Chromodynamics and Local Duality*, Nucl. Phys. B **250**, 61 (1985).
 - [56] E. Braaten, *QCD Predictions for the Decay of the tau Lepton*, Phys. Rev. Lett. **60**, 1606 (1988).
 - [57] E. Braaten, S. Narison, and A. Pich, *QCD analysis of the τ hadronic width*, Nucl. Phys. B **373**, 581 (1992).
 - [58] M. Beneke and M. Jamin, *α_s and the τ hadronic width: fixed-order, contour-improved and higher-order perturbation theory*, JHEP **0809**, 044 (2008) [arXiv:0806.3156 [hep-ph]].
 - [59] D. Boito, P. Masjuan and F. Oliani, *Higher-order QCD corrections to hadronic τ decays from Padé approximants*, JHEP **08**, 075 (2018) [arXiv:1807.01567 [hep-ph]].
 - [60] I. Caprini, *Higher-order perturbative coefficients in QCD from series acceleration by conformal mappings*, Phys. Rev. D **100**, 056019 (2019) [arXiv:1908.06632 [hep-ph]].
 - [61] P. A. Baikov, K. G. Chetyrkin and J. H. Kühn, *Five-Loop Running of the QCD coupling constant*, Phys. Rev. Lett. **118**, 082002 (2017) [arXiv:1606.08659 [hep-ph]].
 - [62] F. Herzog, B. Ruijl, T. Ueda, J. A. M. Vermaseren and A. Vogt, *The five-loop beta function of Yang-Mills theory with fermions*, JHEP **1702**, 090 (2017) [arXiv:1701.01404 [hep-ph]].
 - [63] E. C. Poggio, H. R. Quinn, S. Weinberg, *Smearing the Quark Model*, Phys. Rev. D **13**, 1958 (1976).
 - [64] O. Catà, M. Golterman, S. Peris, *Possible duality violations in tau decay and their impact on the determination of $\alpha(s)$* , Phys. Rev. D **79**, 053002 (2009) [arXiv:0812.2285 [hep-ph]].
 - [65] D. Boito, I. Caprini, M. Golterman, K. Maltman and S. Peris, *Hyperasymptotics and quark-hadron duality violations in QCD*, Phys. Rev. D **97**, 054007 (2018) [arXiv:1711.10316 [hep-ph]].
 - [66] B. Blok, M. A. Shifman and D. X. Zhang, *An illustrative example of how quark-hadron duality*

- might work*, Phys. Rev. D **57**, 2691 (1998) [Erratum, *ibid.* D **59**, 019901 (1999)] [arXiv:hep-ph/9709333].
- [67] I. I. Y. Bigi, M. A. Shifman, N. Uraltsev and A. I. Vainshtein, *Heavy flavor decays, OPE and duality in two-dimensional 't Hooft model*, Phys. Rev. D **59**, 054011 (1999) [hep-ph/9805241].
- [68] M. A. Shifman, *Quark hadron duality*, [hep-ph/0009131].
- [69] M. Golterman, S. Peris, B. Phily and E. de Rafael, *Testing an approximation to large $N(c)$ QCD with a toy model*, JHEP **0201**, 024 (2002) [hep-ph/0112042].
- [70] O. Catà, M. Golterman, S. Peris, *Duality violations and spectral sum rules*, JHEP **0508**, 076 (2005) [hep-ph/0506004].
- [71] O. Catà, M. Golterman, S. Peris, *Unraveling duality violations in hadronic tau decays*, Phys. Rev. D **77**, 093006 (2008) [arXiv:0803.0246 [hep-ph]].
- [72] M. Jamin, *Contour-improved versus fixed-order perturbation theory in hadronic tau decays*, JHEP **0509**, 058 (2005) [hep-ph/0509001].
- [73] M. Beneke, D. Boito and M. Jamin, *Perturbative expansion of tau hadronic spectral function moments and α_s extractions*, JHEP **1301**, 125 (2013) [arXiv:1210.8038 [hep-ph]].
- [74] D. Boito and F. Oliani, *Renormalons in integrated spectral function moments and α_s extractions*, Phys. Rev. D **101**, 074003 (2020) [arXiv:2002.12419 [hep-ph]].
- [75] K. Maltman, *Constraints on hadronic spectral functions from continuous families of finite energy sum rules*, Phys. Lett. B **440**, 367 (1998) [hep-ph/9901239].
- [76] C. A. Dominguez and K. Schilcher, *Chiral sum rules and duality in QCD*, Phys. Lett. B **448**, 93 (1999) [hep-ph/9811261].
- [77] S. Banerjee *et al.*, *Averages of b -hadron, c -hadron, and τ -lepton properties as of 2023*, [arXiv:2411.18639 [hep-ex]].
- [78] J. Erler, *Electroweak radiative corrections to semileptonic tau decays*, Rev. Mex. Fis. **50**, 200 (2004) [hep-ph/0211345].
- [79] R. D. Ball *et al.* [NNPDF], *Fitting Parton Distribution Data with Multiplicative Normalization Uncertainties*, JHEP **05**, 075 (2010) [arXiv:0912.2276 [hep-ph]].
- [80] M. Bruno and R. Sommer, *On fits to correlated and auto-correlated data*, Comput. Phys. Commun. **285**, 108643 (2023) [arXiv:2209.14188 [hep-lat]].
- [81] Y. Schröder and M. Steinhauser, *Four-loop decoupling relations for the strong coupling*, JHEP **01**, 051 (2006) [arXiv:hep-ph/0512058 [hep-ph]].
- [82] K. G. Chetyrkin, J. H. Kühn and C. Sturm, *QCD decoupling at four loops*, Nucl. Phys. B **744**, 121 (2006) [arXiv:hep-ph/0512060 [hep-ph]].
- [83] A. Pais, *The many pi-meson problem*, Ann. Phys. **9**, 548 (1960).
- [84] A. Keshavarzi, D. Nomura and T. Teubner, *$g - 2$ of charged leptons, $\alpha(M_Z^2)$ and the hyperfine splitting of muonium: a new data-based analysis*, Phys. Rev. D **101**, 014029 (2020) [arXiv:1911.00367 [hep-ph]].
- [85] A. Evangelista *et al.* [Extended Twisted Mass], *Inclusive hadronic decay rate of the τ lepton from lattice QCD*, Phys. Rev. D **108**, no.7, 074513 (2023) [arXiv:2308.03125 [hep-lat]].
- [86] See, for instance, O. Helene, *Método dos Mínimos Quadrados com Formalismo Matricial*, Editora Livraria da Física, São Paulo, Brazil, 2006.